



Turbulent rapid mixing in direct filtration  
by Scott Lee Trusler

A thesis submitted in partial fulfillment of the requirements for the degree of Master of Science in Civil Engineering  
Montana State University  
© Copyright by Scott Lee Trusler (1983)

**Abstract:**

The fundamental physical processes which occur in the initial mixing step of coagulation are not fully understood at this time. This work focuses on initial mixing within a direct filtration treatment scheme, in order to gain some insight into the nature of the mixing process. A direct filtration pilot plant incorporating a variable speed, baffled tank mixer was operated with various mixing intensities during the investigation. Filtrate quality and filter head-loss data from the pilot plant were used to establish the effectiveness of a given mixing condition. Also, mixing within a hydraulic jump was similarly investigated in order to compare hydraulic mixing to mechanical (stirred baffled tank or backmix reactor) mixing.

An idealized mixing model, which was based on the interaction of the coagulant carrying turbulent microscales with colloid particles, was proposed. The results of the pilot plant studies indicate that a colloid-microscale size correlation similar to the correlation proposed by the mixing model may exist.

Also, a method was proposed for calculating the mean velocity gradient (G-value) of a hydraulic jump occurring on a sloping channel. The usefulness of this calculation method was confirmed in this study.

Finally, the pilot plant data collected during this investigation indicated that the hydraulic jump was comparable to the baffled tank for initial rapid mixing (based on similar velocity gradients). However, the inflexibility of the hydraulic jump, in regard to variable degrees of mixing, was also evident.

TURBULENT RAPID MIXING  
IN DIRECT FILTRATION

by

Scott Lee Trusler

A thesis submitted in partial fulfillment  
of the requirements for the degree

of

Master of Science

in

Civil Engineering

MONTANA STATE UNIVERSITY  
Bozeman, Montana

May 1983

N378  
T776  
cop. 2

APPROVAL

of a thesis submitted by

Scott Lee Trusler

This thesis has been read by each member of the thesis committee and has been found to be satisfactory regarding content, English usage, format, citations, bibliographic style, and consistency, and is ready for submission to the college of Graduate Studies.

5/27/83  
Date

Ashwathangji  
Chairperson, Graduate Committee

Approved for the Major Department

May 27, 1983  
Date

Theodore Williams  
Head, Major Department

Approved for the College of Graduate Studies

27 May 1983  
Date

Michael Maher  
Graduate Dean

## STATEMENT OF PERMISSION TO USE

In presenting this thesis in partial fulfillment of the requirements for a master's degree at Montana State University, I agree that the Library shall make it available to borrowers under the rules of the Library. Brief quotations from this thesis are allowable without special permission, provided that accurate acknowledgment of the source is made.

Permission for extensive quotation from or reproduction of this thesis may be granted by my major professor, or in his absence, by the director of Libraries when, in the opinion of either, the proposed use of the material is for scholarly purposes. Any copying or use of the material in this thesis for financial gain shall not be allowed without my written permission.

Signature



Date

5-27-83

#### ACKNOWLEDGEMENTS

I wish to express my appreciation to Dr. A. Amirtharajah for his guidance, assistance and encouragement, throughout this investigation.

Also, I wish to thank Mary Mullen, for her assistance during the collection of data, Mrs. Bonnie Recktenwald, who typed this thesis and my family, for their encouragement.

Finally, I am grateful for the support provided by the Engineering Experiment Station at Montana State University and the National Science Foundation/State of Montana MONTS Project, grant No. ISP-8011449.

## TABLE OF CONTENTS

	Page
LIST OF FIGURES . . . . .	vii
LIST OF TABLES . . . . .	ix
NOMENCLATURE . . . . .	x
ABSTRACT . . . . .	xii
1. INTRODUCTION . . . . .	1
2. OBJECTIVES . . . . .	3
3. PREVIOUS RELATED STUDIES . . . . .	4
Turbulent Initial Mixing . . . . .	4
Mixing in baffled tanks . . . . .	5
Mixing in hydraulic jumps . . . . .	8
Mixing in Water Treatment . . . . .	10
Initial mixing studies . . . . .	10
Turbulent flocculation . . . . .	13
Filtration Analysis . . . . .	14
4. IDEALIZED MIXING MODEL . . . . .	16
5. EXPERIMENTAL WORK . . . . .	22
Plan . . . . .	22
Direct Filtration Pilot Plant . . . . .	22
Baffled tank reactor . . . . .	27
Details of flume . . . . .	29
Dual media filter . . . . .	31

TABLE OF CONTENTS--Continued

	Page
Filter Performance Data . . . . .	34
Dye Trace Studies . . . . .	37
6. RESULTS AND DISCUSSION . . . . .	38
Calculated Mixing Parameters . . . . .	38
Velocity gradients . . . . .	38
Hydraulic residence times . . . . .	40
Filtration Results . . . . .	44
Filter response to baffled tank mixing . . . . .	44
Filtrability numbers for baffled tank mixing . . . . .	52
Electrophoretic Mobility Data . . . . .	56
Hydraulic Mixer Comparisons . . . . .	57
7. CONCLUSIONS . . . . .	63
REFERENCES . . . . .	65
APPENDIX - Sample Calculations . . . . .	68

## LIST OF FIGURES

	Page
1. Power Dissipation Zones in a Stirred Tank (Cutter [5]) . . . . .	7
2. Design and Operation Diagram for Alum Treatment . . . . .	12
3. Idealized Colloid-Microscale Interaction Visualization . . . . .	17
4. Schematic Diagram of Direct Filtration Pilot Plant . . . . .	23
5. Size Distributions for Turbidity Particles . . . . .	26
6. Details of Baffled Tank Reactor and Disc- Turbine Impeller . . . . .	28
7. Details of Hydraulic Jump Flume . . . . .	30
8. Details of Dual Media Filter . . . . .	32
9. Residence Time Distributions for the Baffled Tank Reactor . . . . .	41
10. Residence Time Distributions for Two Hydraulic Jumps . . . . .	43
11. Typical Filter Data for Baffled Tank Mixing with Alum Treatment (n = 700 RPM) . . . . .	45
12. Typical Filter Data for Hydraulic Jump Mixing with Ferric Chloride Treatment (Slope = 2.0 in/ft) . . . . .	46
13. Rate of Headloss and Average Effluent Turbidity for Baffled Tank Mixing with Alum Treatment . . . . .	48
14. Rate of Headloss and Effluent Turbidity for Baffled Tank Mixing with Ferric Chloride Treatment . . . . .	49

LIST OF FIGURES--Continued

	Page
15. Rates of Headloss and Average Effluent Turbidity for Baffled Tank Mixing with Ferric Chloride Treatment . . . . .	51
16. Filtrability Numbers for Baffled Tank Mixing with Alum Treatment . . . . .	53
17. Filtrability Numbers for Baffled Tank Mixing with Ferric Chloride Treatment . . . . .	54
18. Filtrability Numbers for Baffled Tank Mixing with Ferric Chloride Treatment . . . . .	55
19. Rates of Headloss for Hydraulic Jump and Open Channel Mixing with Ferric Chloride Treatment . . . . .	59
20. Average Effluent Turbidities for Hydraulic Jump and Open Channel Mixing with Ferric Chloride Treatment . . . . .	61
21. Filtrability Numbers for Hydraulic Jump and Open Channel Mixing with Ferric Chloride Treatment . . . . .	62
22. Hydraulic Jump Length, $L$ , for Jumps in Sloping Channels . . . . .	70

## LIST OF TABLES

	Page
1. Water Analysis of Feed Water for Direct Filtration Pilot Plant . . . . .	24
2. Size Characteristics of Filter Media . . . . .	33
3. List of Pilot Plant Runs Including Coagulant Dosages and pH Conditions . . . . .	36
4. Calculated Velocity Gradients for Baffled Tank Mixer . . . . .	39
5. Calculated Velocity Gradients for Hydraulic Mixers . . . . .	40
6. Mean Hydraulic Residence Times for Baffled Tank Mixer . . . . .	42
7. Electrophoretic Mobility Data for Treatment of M30 and SB325 Colloids . . . . .	58

## NOMENCLATURE

$\bar{C}$	Average effluent turbidity - TU
$C_0$	Filter influent turbidity - TU
$E_T$	Channel flow energy - ft
$F$	Filtrability number
$F_1$	Upstream Froude number for hydraulic jump
$\bar{G}$	Average velocity gradient - $s^{-1}$
$H_T$	Total filter headloss at time T - in
$N_0$	Number of particle collisions
$N$	Number of colloid-microscale interactions
$\bar{P}$	Average power dissipated - $ft \cdot lb/s$
$P_0$	Power number
$Q$	Flow rate - cfs
$Re$	Impeller Reynolds number
$T$	Filter run length - hr
$V$	Power dissipation volume - $ft^3$
$V_r$	Filtration rate - in/hr
$a_1$	Colloid diameter
$d$	Impeller diameter - ft; Water depth in flume-ft
$g$	Acceleration of gravity - $ft/s^2$
$n$	Impeller speed - rev./s
$n_1, n_2$	Colloid number counts
$r_1, r_2$	Colloid radii

NOMENCLATURE--Continued

t	Theoretical mixing time - $V/Q$ - s
u, v, w	Respective velocity components
x, y, z	Respective coordinate directions
$y_2$	Water depth downstream of jump - ft
z	Channel elevation - ft
$\eta$	Microscale
$\epsilon$	Power dissipation per unit mass - $\text{ft}^2/\text{s}^3$
$\gamma$	Specific weight of water - $\text{lb}/\text{ft}^3$
$\mu$	Fluid viscosity - $\text{lb}\cdot\text{s}/\text{ft}^2$
$\nu$	Fluid kinematic viscosity - $\text{ft}^2/\text{s}$
$\rho$	Fluid density - $\text{slugs}/\text{ft}^3$
$\theta$	Flume slope angle

## ABSTRACT

The fundamental physical processes which occur in the initial mixing step of coagulation are not fully understood at this time. This work focuses on initial mixing within a direct filtration treatment scheme, in order to gain some insight into the nature of the mixing process. A direct filtration pilot plant incorporating a variable speed, baffled tank mixer was operated with various mixing intensities during the investigation. Filtrate quality and filter head-loss data from the pilot plant were used to establish the effectiveness of a given mixing condition. Also, mixing within a hydraulic jump was similarly investigated in order to compare hydraulic mixing to mechanical (stirred baffled tank or backmix reactor) mixing.

An idealized mixing model, which was based on the interaction of the coagulant carrying turbulent microscales with colloid particles, was proposed. The results of the pilot plant studies indicate that a colloid-microscale size correlation similar to the correlation proposed by the mixing model may exist.

Also, a method was proposed for calculating the mean velocity gradient ( $\bar{G}$ -value) of a hydraulic jump occurring on a sloping channel. The usefulness of this calculation method was confirmed in this study.

Finally, the pilot plant data collected during this investigation indicated that the hydraulic jump was comparable to the baffled tank for initial rapid mixing (based on similar velocity gradients). However, the inflexibility of the hydraulic jump, in regard to variable degrees of mixing, was also evident.

## CHAPTER 1

## INTRODUCTION

In this day and age, the treatment of water to provide a potable supply for consumers has developed into a multifaceted science incorporating ideas from chemistry, physics and fluid dynamics. Within the overall treatment picture, certain processes and treatment methods have received considerable attention over the past decade. Direct filtration, which is filtration not preceded by sedimentation, is one treatment scheme where attention has been focused. Another aspect which has received considerable attention is that of chemical reactions within agitated vessels. In particular, the role of the mixing intensity itself within the overall chemical process is of considerable interest.

In addition to the agitated vessel mixing mentioned above, turbulent hydraulic mixing has also received some attention. The usefulness of the hydraulic jump for mixing in water treatment has, however, not been recently studied. A rational design procedure for the hydraulic jump is important for several reasons. First of all, hydraulic jump mixing is operationally simplistic which leads to high reliability. Also, hydraulic mixers usually require less total power input than mechanical mixers which

further enhance their operational attractiveness. The reason for the lower power requirements are two fold. First, the power dissipation volumes for hydraulic mixers are usually much smaller than the volumes for mechanical mixers. Secondly, hydraulic mixers lack the frictional inefficiencies common to motor driven mixers. There is no doubt that hydraulic mixing has its share of drawbacks as well. The primary disadvantage, with the hydraulic jump being the inability to change the mixing intensity to accomodate variations in the influent water quality.

The present study focused on initial mixing within a direct filtration treatment scheme. Both mechanical (stirred baffled tank) and hydraulic (hydraulic jump) mixing were investigated. The importance of this study was based on the need for a better understanding of the initial mixing step of coagulation. This better understanding will, no doubt, lead to more efficient use of the energy employed in water treatment mixing operations.

## CHAPTER 2

## OBJECTIVES

The overall objective of this study was to investigate the initial mixing step of coagulation and to gain some insight into the fundamental nature of the mixing process. The following were the specific objectives:

1. To study the initial mixing step of coagulation in a stirred baffled tank reactor in order to determine the role of mixing intensity in destabilization by charge neutralization using a direct filtration pilot plant.
2. To attempt to relate the results of the mixing study to the microscale of turbulence.
3. To propose a methodology for design of hydraulic jump mixers.
4. To compare hydraulic jump mixing with baffled tank (backmix) reactor mixing.

## CHAPTER 3

## PREVIOUS RELATED STUDIES

The theoretical studies which are related to this work can be divided into three categories. First, there is the material which deals with turbulence and mixing in general. Second, are the studies which have focused on mixing in the water treatment field. Both flocculation and initial mixing studies are of importance here. Finally, some aspects regarding filtration analysis will be presented.

TURBULENT INITIAL MIXING

As defined by Hinze [1], turbulence is a flow condition characterized by irregular motion in which various parameters vary in time and space. Hinze also points out that within the random variations, statistically distinct averages are obtainable. The concepts underlying turbulence, such as fluctuating velocities and turbulent intensities, are fully developed in the literature [1, 2] and will not be discussed here. Of more concern to the present study, are the fundamentals of energy dissipation within a turbulent flow.

In any given turbulent flow it can be shown that regions of high velocity correlation exist. In a somewhat rough approximation, these regions where all the fluid exhibits

a similar velocity can be interpreted as eddies or vortices. Kolmogoroff [3,4] was the first to rationalize turbulence from an eddy or length scale viewpoint by defining an integral length scale and a microscale. The integral scale is related to large eddies which carry energy and the microscale is the eddy size at which energy dissipation by viscous friction begins. Kolmogoroff noted that these small eddies (microscale) would have to be in a state of equilibrium and their size would be a function of the energy input and the fluid viscosity. By dimensional analysis Kolmogoroff quantified the microscale as

$$\eta = \left( \frac{\nu^3}{\varepsilon} \right)^{0.25} \quad (1)$$

where  $\eta$  is the microscale,  $\nu$  is the kinematic viscosity of the fluid and  $\varepsilon$  is the power dissipated per unit mass. Since mixing is usually interpreted as being a function of power dissipation, it is the turbulent microscale which is of particular importance here.

#### Mixing in Baffled Tanks

Several ideas in regard to mixing in baffled tanks are important to this investigation. First there are the results of Cutter [5] which illustrate the nonuniformity of power dissipation within a baffled tank. Cutter found three distinct regions of power dissipation to exist within a

baffled tank. He labeled the regions as the tip zone, the impeller stream zone and the bulk zone. Figure 1 illustrates the three zones and the approximate power dissipation within each zone, in relation to the mean dissipation. More recently, Okamoto, Nishikawa and Hashimoto [6] have confirmed the existence of the impeller stream and bulk zones of a baffled tank as described by Cutter.

Long before Cutter's work, Camp and Stein [7] formulated the velocity gradient, or G-value, as a design parameter for determining the power requirements of a mixer. Camp and Stein utilized laminar fluid shear concepts to derive the velocity gradient as

$$\bar{G} = \left( \frac{\bar{P}}{\mu V} \right)^{0.5} \quad (2)$$

where  $\bar{G}$  is the average velocity gradient,  $P$  is the power dissipated within volume  $V$  and  $\mu$  is the fluid viscosity. Camp and Stein also generalized the velocity gradient expression for turbulent flows by defining the root mean square (RMS) velocity gradient as

$$G = \left[ \left( \frac{\partial u}{\partial y} + \frac{\partial v}{\partial x} \right)^2 + \left( \frac{\partial v}{\partial z} + \frac{\partial w}{\partial y} \right)^2 + \left( \frac{\partial w}{\partial x} + \frac{\partial u}{\partial z} \right)^2 \right]^{0.5} \quad (3)$$

where  $u$ ,  $v$  and  $w$  are the velocities in the  $x$ ,  $y$  and  $z$  directions respectively. Equation (2) thus represents an average value within a turbulent field.

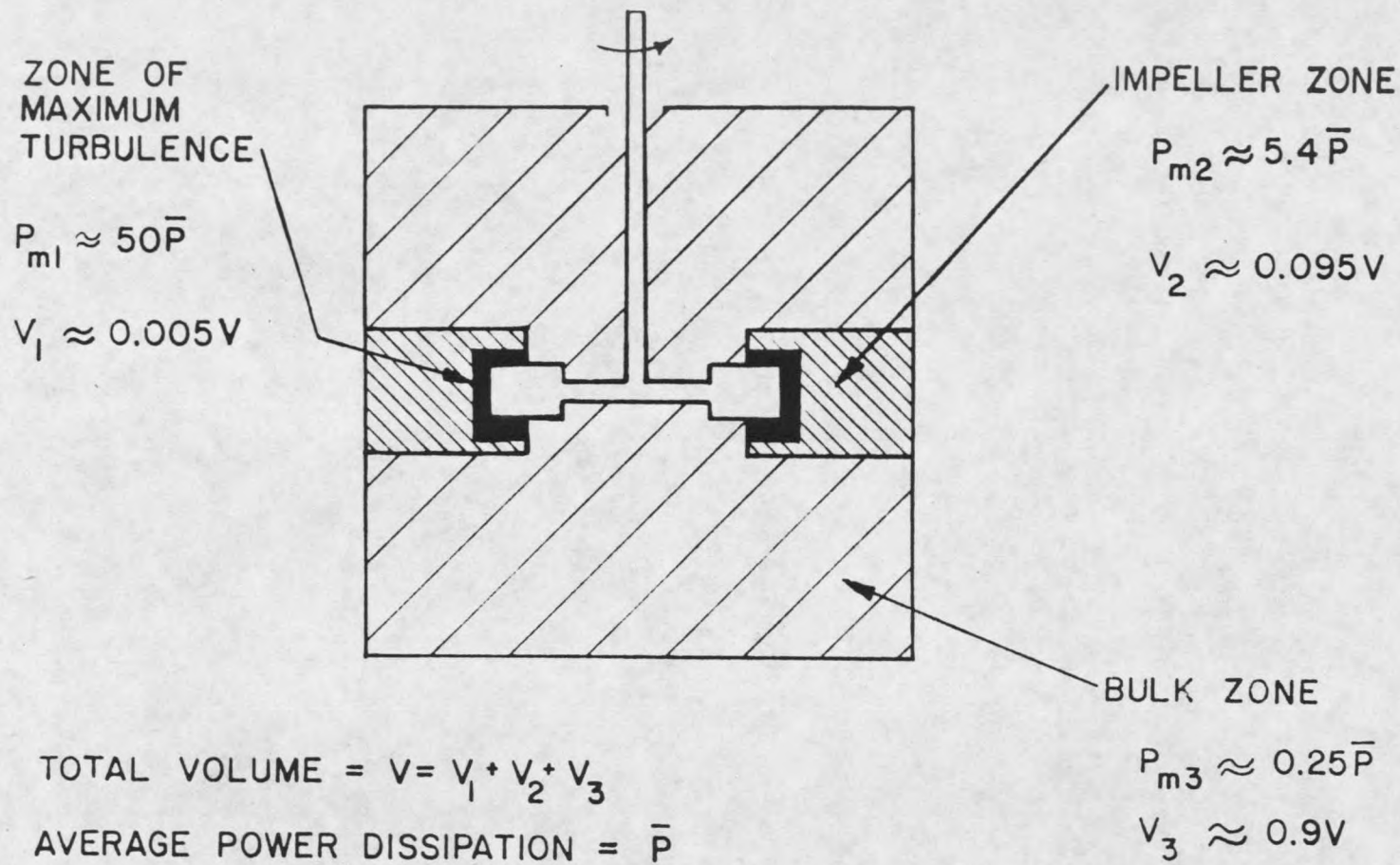


FIGURE 1. Power Dissipation Zones in a Stirred Tank (Cutter [5]).

Another parameter which is important in tank mixing is the dimensionless power number,  $P_o$ . Leentvaar and Ywema [8] explain the power number concept in detail and show the quantified expression as

$$P_o = \bar{P} \rho^{-1} n^{-3} d^{-5} \quad (4)$$

where  $\bar{P}$  is again the average power dissipated,  $\rho$  is the density of the fluid,  $n$  is the impeller speed and  $d$  is the impeller diameter. For a given reactor-impeller configuration, the power number remains constant beyond a certain Reynolds number  $Re$  ( $\approx 10^4$  for cylindrical baffled tanks) where

$$R_e = \left( n \frac{d}{\nu} \right)^2 \quad (5)$$

and all symbols are as previously defined. Thus, once the power number of a given reactor is known, power inputs and corresponding G-values can be computed for various impellers and rotation speeds.

#### Mixing in Hydraulic Jumps

At present, mixing in hydraulic jumps is somewhat less well defined than mixing in baffled tanks. Chow [9] presents all the tools necessary to formulate a possible design rationale. The hydraulic jump can be defined as the mechanism by which an open channel flow transforms from supercritical

to subcritical flow. Looking at the mixing capabilities of the jump from a  $\bar{G}$ -value standpoint, necessitates that the power dissipated within a specific volume be related to the jump characteristics.

Power dissipation in a hydraulic jump is actually well understood and the mechanism is undoubtedly turbulence. Theory pertaining to energy losses in a jump is derived in detail by Chow for both mild and steep channels. Actual energy losses are easily computed from water depth measurements in the vicinity of the jump, since

$$E_T = z + d\cos\theta + \frac{v^2}{2g} \quad (6)$$

where  $E_T$  is the total flow energy,  $z$  is the channel elevation,  $d$  is the water depth,  $\theta$  is the slope angle,  $v$  is the flow velocity and  $g$  is the acceleration due to gravity. Thus, by computing  $E_T$  upstream and downstream of the jump, the loss of energy in the jump can be estimated. Then utilizing the expression for power

$$\bar{P} = \gamma Q(\Delta E_T) \quad (7)$$

where  $\gamma$  is the specific weight of water, and  $Q$  is the flow rate and  $E_T$  is the energy lost in the jump, the average power dissipated in the jump,  $P$  is determined as well.

The volume in which the power dissipation occurs is most likely related to the characteristic jump length.

Chow illustrates that the jump length  $L$  is a function of the available flow energy (upstream Froude number and channel slope) and presents empirical data which can be used to estimate the length of a jump which occurs in a sloping channel. The actual power dissipation can then be assumed to occur in the fluid volume contained in the jump length  $L$ . Since the power and dissipation volume are known, a  $\bar{G}$ -value for the jump can be computed.

#### MIXING IN WATER TREATMENT

Mixing studies within the water treatment field are numerous, however, only a few studies are relevant here. These relevant investigations may be split into those which have dealt with initial rapid mixing directly and those which have dealt with flocculation.

#### Initial Mixing Studies

Wilson [10] attempted to define optimum rapid mixing by studying the flocculation efficiencies resulting from two different mixing methods. The actual optimization was based on a floc strength model where optimum mixing was defined as the condition which produced the strongest flocs within the flocculator. Wilson employed a baffled tank reactor and a tubular reactor in his studies and concluded that uniform, instantaneous, plug-flow mixing was the optimum condition based on floc strength.

Sometime later, Stenquist and Kaufman [11] completed a series of continuous flow experiments in which they compared a flash mixer (backmix) to a multiple orifice grid mixer (pipe flow). Their results produced no conclusive evidence that backmixing was inherently inferior to plug-flow mixing for alum treatment, when flocculation efficiency was used as the gauge. Even though Stenquist and Kaufman's conclusions seem to contradict those of Wilson, the results of both studies may have been more a function of alum coagulation chemistry than of mixing itself. The actual effects of alum dosage in relation to mixing are discussed below.

Amirtharajah and Mills [12] developed the design diagram for alum treatment as shown in Figure 2. The diagram is based on thermodynamic principles and delineates the region of solid phase aluminum hydroxide as a function of pH. Also shown on the diagram are regions where specific coagulation mechanisms predominate. Amirtharajah and Mills then applied the diagram to rapid mixing by performing jar tests with various degrees ( $\bar{G}$ -values) of rapid mixing. They concluded that intense, short duration mixing was essential if adsorption-destabilization was the primary mechanism of coagulation. They also found that when sweep coagulation was the predominant mechanism, mixing effects were minimal. It is important to note, that Wilson and Stenquist both operated

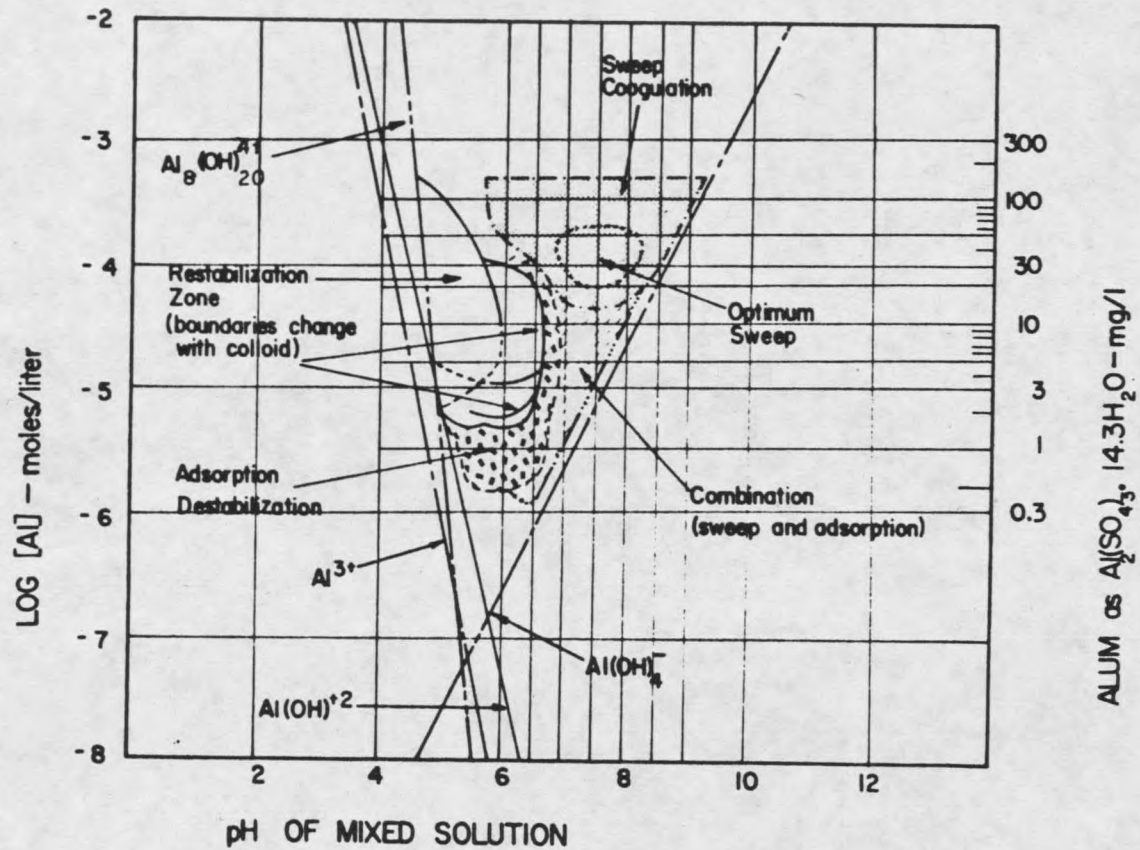


FIGURE 2. Design and Operation Diagram for Alum Treatment.

their mixers in the sweep zone during their investigations. Amirtharajah [13] also suggested that a fundamental size relationship between the turbulent microscale and the particles which were to be destabilized may exist.

Only one investigation of the hydraulic jump's effectiveness as an initial mixer has been reported. Levy and Ellms [14] conducted full scale alum treatment studies utilizing a hydraulic jump for rapid mixing. They concluded that the hydraulic jump was a very effective means for mixing coagulants. For the energy expended, Levy and Ellms concluded that the jump produced mixing of great rapidity and thoroughness.

#### Turbulent Flocculation

Of primary importance to this investigation are particle collision theories which were first introduced by von Smoluchowski [15]. He derived the collision theories for laminar shear but the original formulations have now been generalized for turbulent flow conditions. Saffman and Turner [16] utilized Smoluchowski's ideas to predict the collision of rain droplets in a turbulent cloud. They quantified the number of collisions,  $N_o$ , as

$$N_o = n_1 n_2 (r_1 + r_2)^3 \left( \frac{8\pi\epsilon}{15\nu} \right)^{0.5} \quad (8)$$

where  $n_1$  and  $n_2$  are respective drop number counts,  $r_1$  and  $r_2$  are respective drop radii, and all other symbols are as previously defined. Spielman [17] has also pointed out that Saffman and Turner's Equation (8) is applicable to turbulent flocculation. Most recently, Adler [18] has incorporated Smoluchowski's ideas into a general particle collision theory which incorporates hydrodynamic effects as well as electric field, double layer and Van der Waals' forces. He subdivides coagulation into homocoagulation and heterocoagulation, where homo- refers to coagulation of equal-sized particles and hetero- refers to coagulation of unequal-sized particles. Adler concluded that homocoagulation is almost always better, at least within the chemical and physical constraints of his development. Considering all the above studies, von Smoluchowski's ideas, and their extension to turbulent flow, seem to be far reaching and may thus be applicable to the rapid mixing process.

#### FILTRATION ANALYSIS

Since this study is not an investigation of filtration fundamentals per se, the only literature of interest is that which deals with analysis of filtration data. The overall response of a filter to the deposition of mass within the media is a function of both headloss and effluent quality. Several researchers have attempted to define the response of a filter to mass loading by combining headloss and efflu-

ent quality data into a single filtrability index [19, 20, 21, 22, 23]. Recently, Janssens, Adam and Buekens [24] did a statistical analysis on various filtrability indexes utilizing direct filtration pilot plant data as a base. They were interested in determining which index would be the best tool for filter response analysis. They concluded that the Filtrability Number, proposed by Ives [21], was the most useful. The expression for the Filtrability Number  $F$ , is given by

$$F = \frac{H_T \bar{C}}{C_0 V_r} \quad (9)$$

where  $T$  is the filter run length defined by effluent quality degradation,  $H_T$  is the total headloss at time  $T$ ,  $\bar{C}$  is the average filter effluent turbidity through time  $T$ ,  $C_0$  is the filter influent turbidity and  $V$  is the filtration rate. Consistent units make  $F$  a dimensionless parameter. Close inspection of the arrangement of the individual parameters in the expression for  $F$ , leads to the conclusion that when  $F$  is minimized, an optimum filtration condition exists.

## CHAPTER 4

## IDEALIZED MIXING MODEL

The first step in developing an idealized mixing model involved a visualization process whereby the microscopic aspects underlying mixing could be postulated. Since mixing is most often associated with power dissipation, interactions between colloid particles in suspension and the turbulent microscale can be rationalized as being of primary importance. The visualization was confined to a homogeneous turbulent field consisting of eddies whose size could be represented by the microscale formulation (1). Also, the development was restricted to the adsorption-destabilization process where a uniform particle suspension was to be treated with a chemical coagulant. Furthermore, the microscale eddies in the field were assumed to be responsible for the transport of the coagulant hydrolysis species, which are most likely in incipient form.

Turning to the visualization, Figure 3 illustrates two simplistic particle-microscale interaction possibilities. Case 1 represents a condition where the microscale is much larger than the colloids and thus, the particles are imbedded within the eddy. Particles in the eddy will experience a laminar like shear field and are also exposed to the coagu-

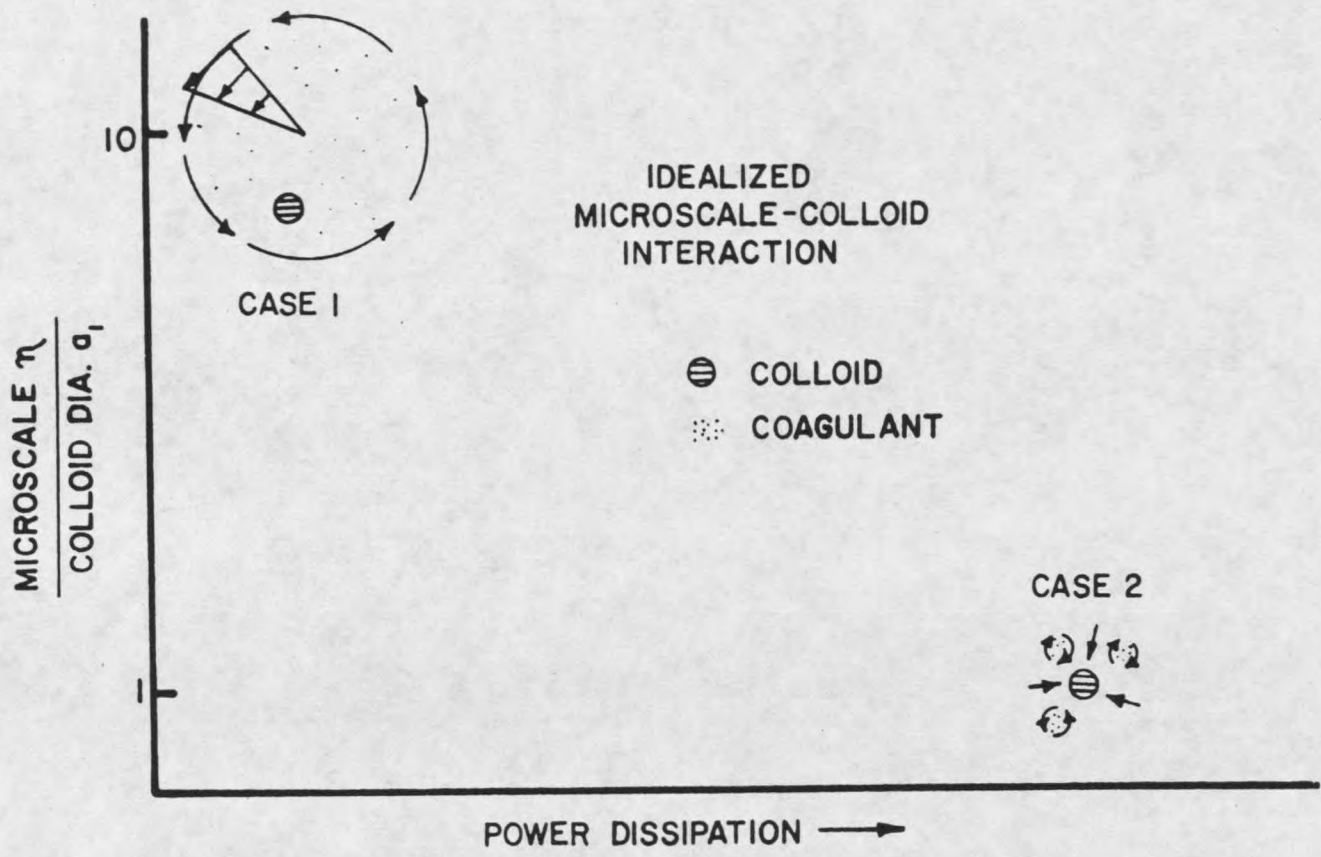


FIGURE 3. Idealized Colloid-Microscale Interaction Visualization.

lant. Under the conditions of Case 1, the efficiency of the rapid mix (based on destabilization) would seem to be controlled by the coating mechanisms which cause the coagulant to be adsorbed onto the colloid. The exact nature of the coating mechanisms is presently not fully understood.

As more power is made available to the system, a transition is made to smaller and smaller eddies. Finally, the condition exists where the microscale and colloids are equal in size and this condition is shown as Case 2 in Figure 3. The Case 2 condition is such that the particles and eddies can be considered as separate entities and in order for the colloids to be exposed to the coagulant, a collision of sorts must occur. Thus, the efficiency of mixing in the Case 2 situation may be controlled by a collision or interaction phenomenon.

In looking more closely at the transition zone between Case 1 and Case 2, Amirtharajah [25] has proposed the following colloid-microscale interaction theory. The basis of the idea was that for colloid destabilization to occur, the colloid particles must be coated with the positively charged aluminum hydroxide solid phase species which are incipiently formed in the fluid. These species have to be transported by the fluid eddies so that they will interact with the colloid particles.

Starting with Saffman and Turner's Equation (8), which is applicable for the condition where the turbulent microscale is larger than the particles and with some minor rearrangement,

$$N = kn_1n_2(a_1 + \eta)^3\left(\frac{\epsilon}{\nu}\right)^{0.5} \quad (10)$$

where  $N$  is the number of colloid-microscale interactions,  $k$  is a constant,  $a_1$  is the colloid diameter,  $\eta$  is the microscale,  $\nu$  is the fluid kinematic viscosity,  $\epsilon$  is the power dissipation per unit mass and  $n_1$  and  $n_2$  are the colloid and microscale number counts respectively. Within a given mixer, the number count of colloids can be considered constant. Furthermore, in this first approximation model, the number count of microscale eddies is assumed constant, even though there is little doubt that as the size of the microscale is reduced, the number count of eddies will increase within the mixing volume. With the above assumptions, Equation (10) is reduced to the form

$$N = k_1(a_1 + \eta)^3\left(\frac{\epsilon}{\nu}\right)^{0.5} \quad (11)$$

Rearranging the microscale expression, Equation (1), in the form

$$\varepsilon = \left(\frac{v}{\eta}\right)^3 \quad (12)$$

and substituting into Equation (11) yields

$$N = k_1 v (a_1 + \eta)^3 \left(\frac{1}{\eta}\right)^2 \quad (13)$$

The fluid viscosity is assumed to be independent of  $\eta$  and is, therefore, incorporated into the constant yielding

$$N = k_2 (a_1 + \eta)^3 \left(\frac{1}{\eta}\right)^2 \quad (14)$$

as the proposed mixing theory expression.

In order to identify the extreme points of the mixing theory, Equation (14) was expanded and differentiated with respect to  $\eta$  giving

$$\frac{dN}{d\eta} = -k_2 \left[ 2 \left(\frac{a_1}{\eta}\right)^3 + 3 \left(\frac{a_1}{\eta}\right)^2 - 1 \right] \quad (15)$$

Setting Equation (15) equal to zero leads to

$$2\left(\frac{a_1}{\eta}\right)^3 + 3\left(\frac{a_1}{\eta}\right)^2 - 1 = 0 \quad (16)$$

and a real root of  $(a_1/\eta) = 0.5$ . Taking the second derivative of Equation 14,

$$\frac{d^2N}{d\eta^2} = 6k_2(a_1^3\eta^{-4} + a_1^2\eta^{-3}) \quad (17)$$

and substituting  $a_1 = 0.5\eta$  gives a positive value for Equation (17) for all  $\eta$  indicating a minimum for Equation 14. Thus, when the microscale is twice the colloid size a minimum number of colloid-microscale interactions should occur.

Although the above derivation is not complete or rigorous, as a first approximation, it provides some interesting insights into the initial mixing process.

## CHAPTER 5

## EXPERIMENTAL WORK

PLAN

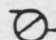
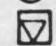
The experimental portion of this study consisted primarily of measuring the response of a dual media filter to various methods of rapid mixing the coagulant. Both mechanical and hydraulic mixing were utilized during the investigation. A baffled tank reactor served as the mechanical mixer and hydraulic mixing was provided by a flume apparatus. Mixing within the flume was produced by either turbulent open-channel flow or a hydraulic jump.

The sensitivity of a dual media filter to small changes in the characteristics of its influent suspension is well known [26]. Thus, the filter makes an ideal gauge for measuring the effectiveness of the rapid mix.

DIRECT FILTRATION PILOT PLANT

A direct filtration pilot plant was constructed in order to study the initial mixing step of coagulation. Figure 4 illustrates the pilot plant flow scheme. A constant flow of 2.0 gpm (8 gpm/ft<sup>2</sup> filtration rate) was maintained through all pilot plant runs. Both hot and cold tap water were used to insure constant temperature conditions. A Powers Foto-

- A. THERMAL BLENDING VALVE
- B. 20 MICRON FILTER
- C. RAW WATER PREPARATION
- D. BUFFER FEED
- E. TURBIDITY FEED
- F. COAGULANT FEED
- G. RAPID MIXER
- H. DUAL MEDIA FILTER

-  PUMP
-  FLOW METER

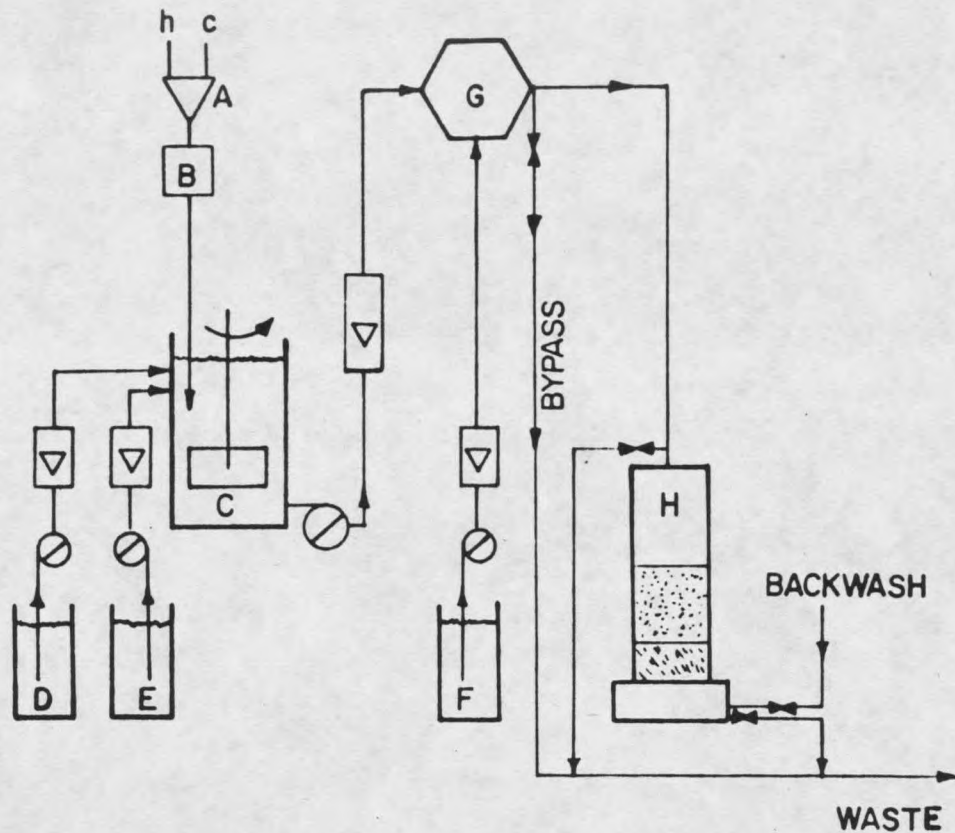


FIGURE 4. Schematic Diagram of Direct Filtration Pilot Plant.

guard Model 440-1500 thermostatic blending valve mixed the hot and cold streams to provide the constant temperature feed water. The temperature of the feed water was 80°F for all plant runs. A chemical analysis of the feed water was performed during the investigation and the results are listed in Table 1.

Table 1. Water Analysis of Feed Water for Direct Filtration Pilot Plant.

PARAMETER	QUANTITY
Total Hardness	105 mg/l as CaCO <sub>3</sub>
Total Alkalinity	80 mg/l as CaCO <sub>3</sub>
Total Dissolved Solids	150 mg/l
Turbidity	0.5 to 1.0 TU
pH	7.4 - 7.7
SO <sub>4</sub> <sup>-2</sup>	8.0 mg/l
PO <sub>4</sub> <sup>-3</sup>	<0.2 mg/l

None of the analysis results are particularly significant except for the sulfate concentration of 8.0 mg/l. Sulfate concentrations of 8.0 mg/l and up have been shown to have a considerable impact on the effectiveness of alum when it is used as a coagulant. It is believed that the sulfate anion neutralizes the charge on the aluminum hydroxide solid phase which greatly reduces its destabilization potential [27].

The remainder of the raw water preparation was carried out in a 20 gallon continuously stirred tank. The raw water tank was fed continuously with the constant temperature feed water as well as a turbidity slurry and pH buffer solution.

Hydrochloric acid (Baker Reagent, 37% HCl), at a concentration of 30 milliliters acid per liter of water, was used for the buffer solution. Feeding the buffer into the raw water tank provided a near constant raw water pH through all plant runs.

A suspension of Min-U-Sil ( $\text{SiO}_2$ ) was used for the turbidity slurry. Two different particle size distributions were used in the experimental work and Figure 5 illustrates the distributions. It is important to note that distributions by weight as well as distributions by particle numbers are shown in Figure 5. The weight distributions were obtained by standard hydrometer tests (ASTM D422). An Omnimet Image Analyzer (IA) by Buehler (Bausch & Lomb) was employed to provide the number count distributions. The IA consists of a microscope which is coupled to a visual monitor. The IA's electronics scan for shading differentiation (particles against background) and then count the particles which are greater than a specified size.

Samples for the IA were diluted samples of the turbidity slurry. The IA samples were analyzed in suspension form because drying the samples caused particles to agglomerate which led to erroneous results.

The Min-U-Sil material itself is a product of the Pennsylvania Glass Sand Corporation (PGS). Min-U-Sil 30 (M30), the coarsest grind manufactured by PGS, served as one of

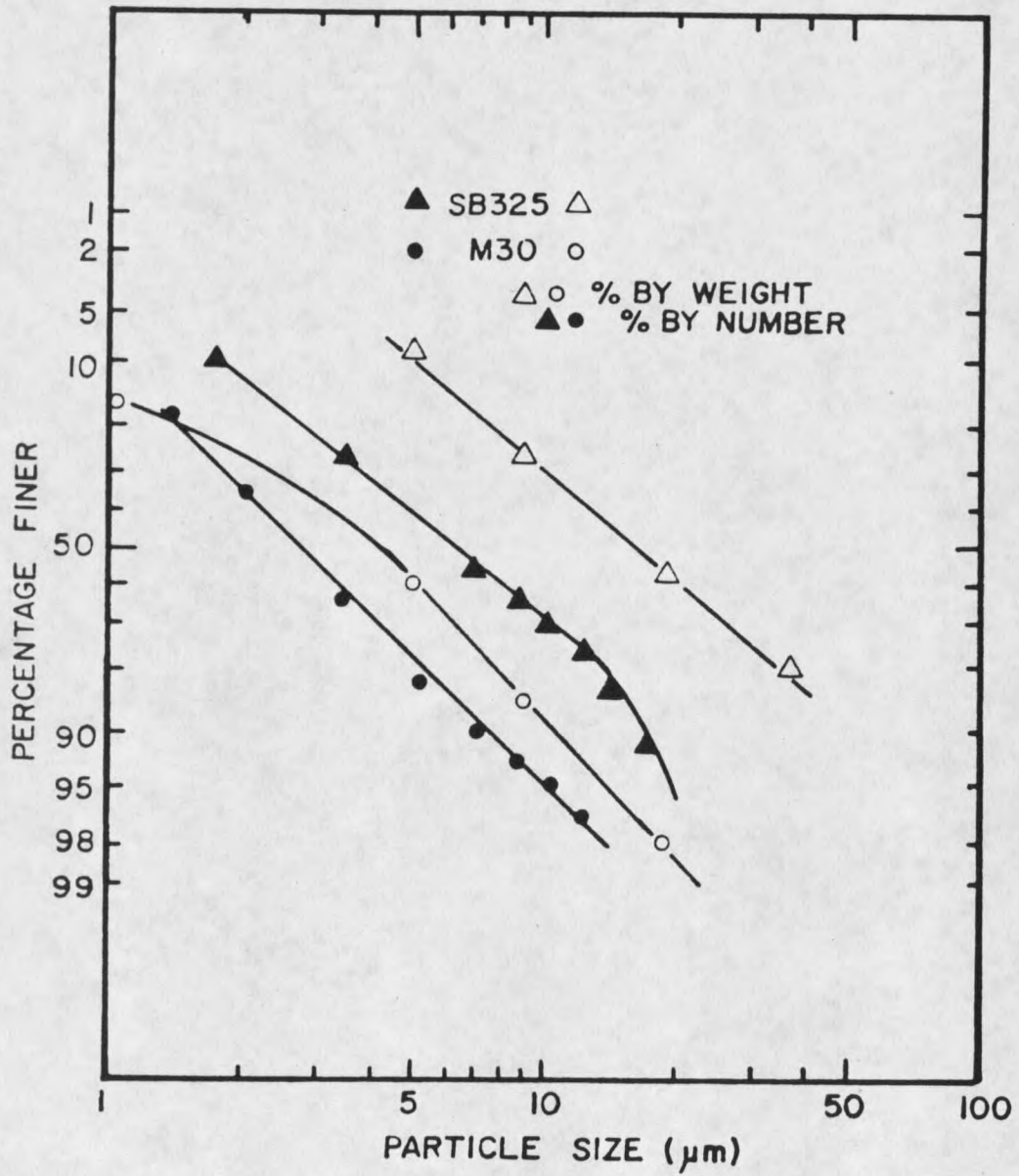


FIGURE 5. Size Distributions for Turbidity Particles.

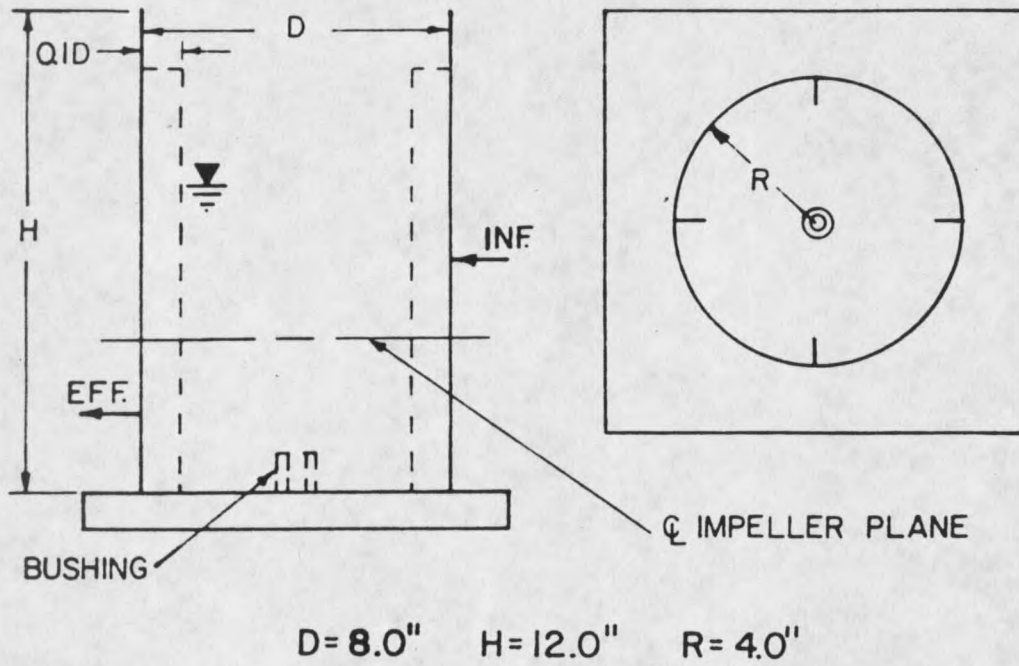
the particle distributions. The other distribution, SB325, was obtained from Berkeley 325 which is the feed stock for the M30 grinding mills. A sedimentation process, outlined below, was employed to produce the SB325 from the Berkeley 325 material.

Suspensions of 50 grams per liter of Berkeley 325 were prepared in 5 gallon buckets and allowed to sit for one hour. The particles which settled in this time period were collected and dried resulting in the SB325 distribution. This sedimentation process was developed based on the ASTM D422 hydrometer test and was designed to remove a major fraction of the particles smaller than 5 micrometers.

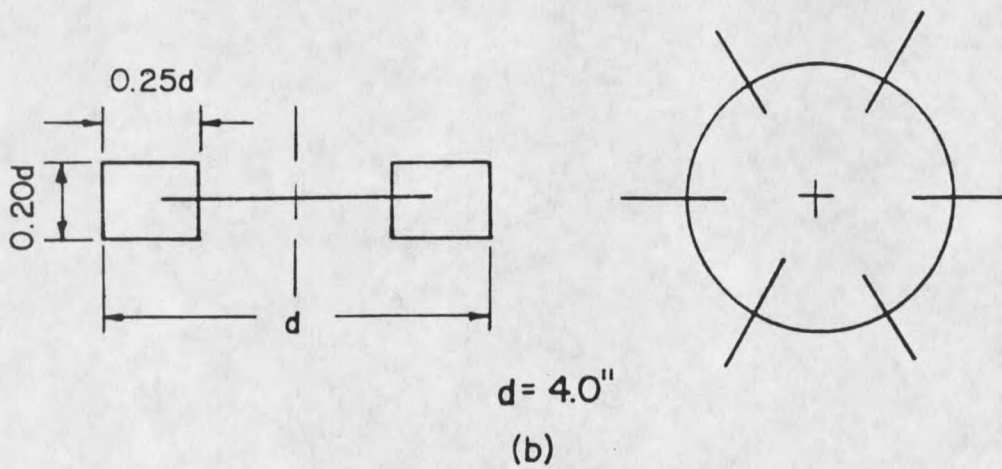
From the raw water tank, the water proceeded to the rapid mix unit where either alum ( $\text{Al}_2(\text{SO}_4)_3 \cdot 16\text{H}_2\text{O}$ ) or ferric chloride ( $\text{FeCl}_3 \cdot 6\text{H}_2\text{O}$ ) was introduced to destabilize the suspension by charge neutralization. After rapid mixing, the destabilized suspension passed directly into the dual media filter. The details of each of the rapid mix units, as well as the details of the filter, are described below.

#### Baffled Tank Reactor

Based on the designs of other research [5, 6, 8] and scale up considerations, the baffled tank reactor was constructed as shown in Figure 6. Also shown in Figure 6 are the details of the disc turbine impeller which was used for mixing in the baffled tank. Both the tank and the



(a)



(b)

FIGURE 6. Details of Baffled Tank Reactor and Disc-Turbine Impeller.

impeller were constructed of plexiglas.

A constant water depth of 8.0 inches was maintained in the reactor during all pilot plant runs. The influent to the reactor was fed 6.0 inches above the reactor bottom and the effluent was drawn off 2.0 inches above the bottom. This reactor configuration forces all the flow to pass through the impeller plane center line which was 4.0 inches above the bottom. The coagulant was fed into the reactor system on the impeller plane center line at a point 0.25 inches from the blade tips. A Bodine NHS-54 variable speed motor was used to drive the impeller.

#### Details of Flume

As a comparison for the baffled tank, a hydraulic mixing device which incorporated a narrow flume and a hydraulic jump was constructed. Figure 7 illustrates the flume configuration and all important dimensions. Various channel slopes could be attained by adjusting the position of a sliding block on the aluminum base. Slopes of 1.5, 2.0, 2.5 and 3.5 inches per foot were utilized in the experiments. These slopes produced highly turbulent, supercritical flow conditions within the channel. By inserting a barrier in the channel, which essentially acted as a sluice gate, a hydraulic jump could be produced.

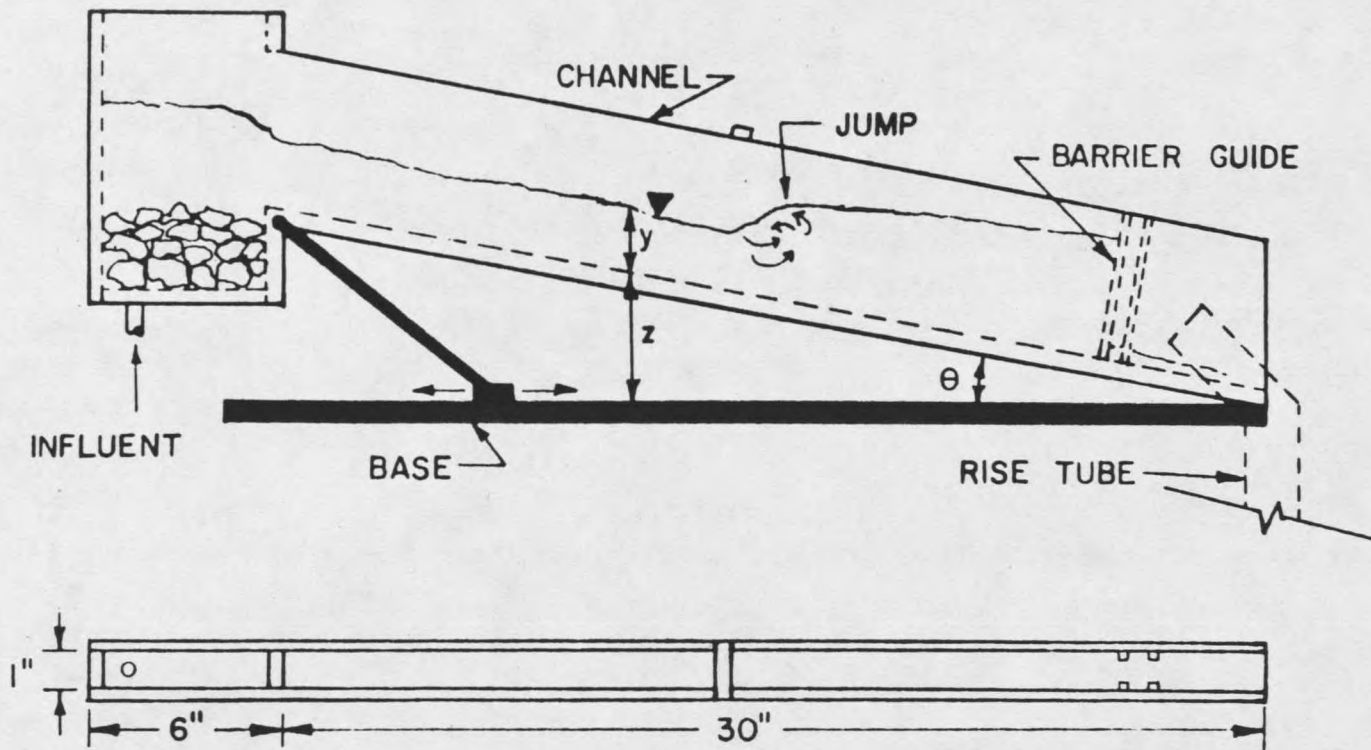


FIGURE 7. Details of Hydraulic Jump Flume.

The flume-jump apparatus was placed in exactly the same location as the baffled tank within the overall plant scheme. Raw water entered the channel via a stilling basin filled with stones to disperse the flow. Once the water passed into the channel section it was destabilized by the addition of the coagulant. When a hydraulic jump was being used, the coagulant feed point was approximately 1.5 inches upstream of the jump toe. During plant runs where the channel flow alone provided the mixing, the coagulant feed point was midway along the channel length. It should be noted, that the flume was used to treat the M30 suspension only. Finally, the destabilized suspension passed directly into the filter rise tube as shown in Figure 7.

#### Dual Media Filter

Since the response of the filter was to be used as the principal method of determining mixing effectiveness, the filter itself was carefully designed. An overall schematic of the filter is shown in Figure 8. The effluent from the rapid mixer enters the filter via a 2.0 inch diameter rise tube. As the filter media clogs during a run, the water level in the rise tube increases, thus providing constant rate filtration with influent control. The filter media consisted of 16 inches of anthracite coal over 8.0 inches of silica sand.

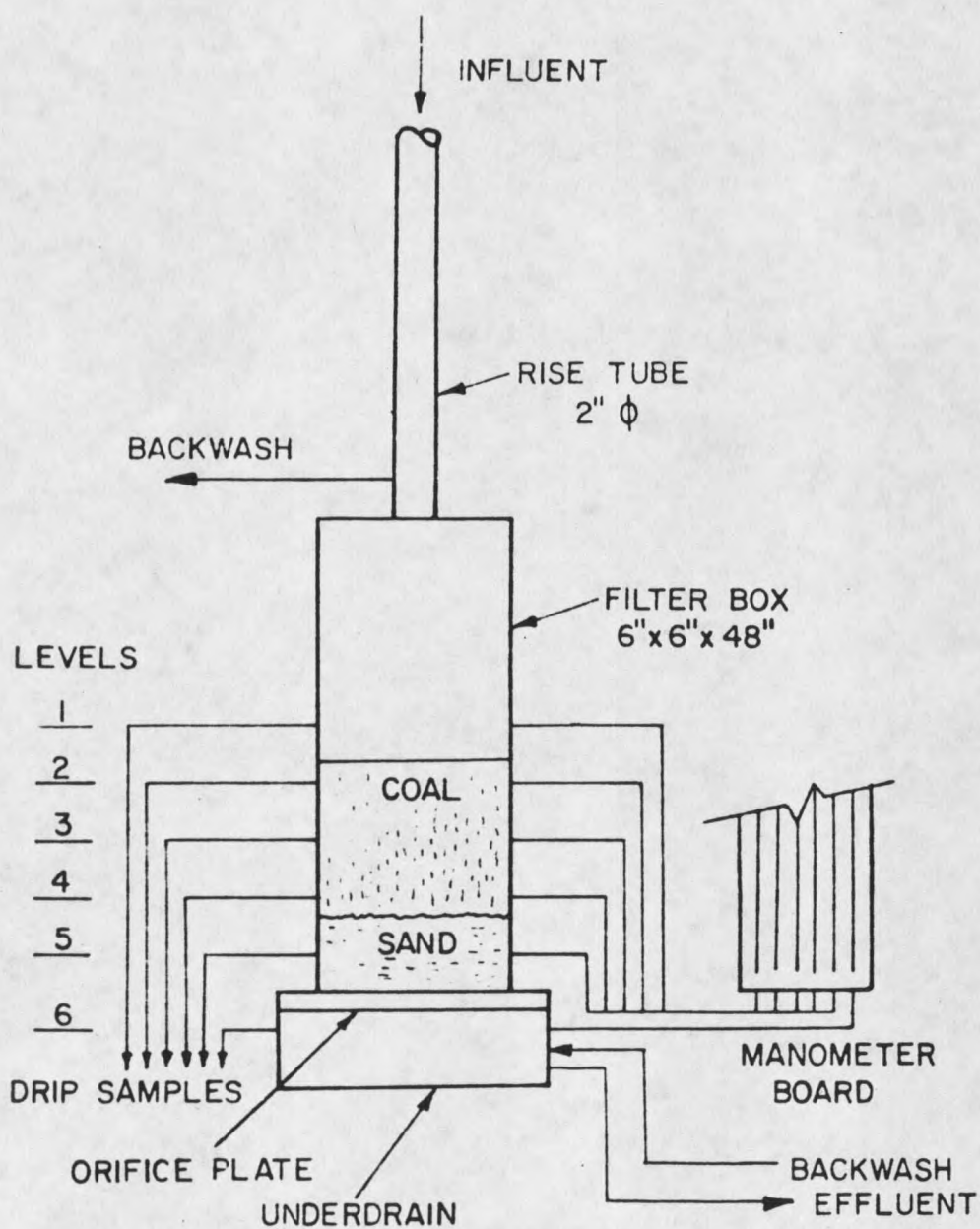


FIGURE 8. Details of Dual Media Filter.

Table 2. Size Characteristics of Filter Media.

SIZE CHARACTERISTIC	SAND	COAL
D <sub>10</sub> (mm) (Effective Size)	0.46	0.86
D <sub>60</sub> (mm)	0.62	1.25
D <sub>90</sub> (mm)	0.70	1.52
Uniformity Coefficient	1.35	1.46

Table 2 lists the size characteristics of the sand and coal media. The media sizes were carefully chosen, based on literature [28] guidelines, to insure a good zone of inter-mixing and compatible expansion characteristics.

A 6x6x48 inch plexiglas column served as the filter box. This configuration (6x6 inch) provided 0.25 square feet of filter surface which yielded a filtration rate, based on a plant flow of 2.0 gpm, of 8 gpm/ft<sup>2</sup>. The box was divided into five levels with a continuous-drip turbidity sampler and manometer port placed at each of the five levels. Level one was 25 inches above the orifice plate (1 inch above the media) and the successive lower levels were spaced at 5 inch intervals. Also, a sixth level was established below the orifice plate to collect effluent turbidity and total headloss data. The drip sampler consisted of an aluminum tube extending into the center of the filter box. The manometer ports were similarly constructed but

only projected 0.5 inches into the media. A plexiglas plate with twenty five 0.25 inch diameter holes was used for the orifice plate. The function of the orifice plate was to support the media (in addition to a nylon mesh) and to provide even filtration. Also, the orifice plate provided even dispersion of the backwash water during cleaning.

Cleaning of the filter was systematically performed by using both air scour and water backwash. Air was blown into the submerged filter media through each of the drip samplers. The necessity for air scour was established after water washing alone proved to be ineffective in breaking up the chunks of material which were sheared off the media. After the air flow was stopped, the filter was washed with water for an extended period of time. The washing flow rate employed was sufficient to provide a fifty percent expansion of the bed.

#### FILTER PERFORMANCE DATA

To insure the stability of the pilot plant and to determine the filter response, various physical and chemical parameters were recorded at half hour intervals throughout each run. Measurements of pH were made on the raw water and filter effluent (level 6) in order to maintain constant chemistry within the flow system. An Altex digital pH meter from Beckman Instruments was used for all the pH measurements. Also, the raw water turbidity was monitored to insure constant mass loading of the rapid mixer and filter.

Filter response to the various rapid mix conditions was established by recording the turbidity of the water from each of the drip samplers. In addition to the turbidity data, headloss data was obtained by monitoring the total available head at each level in the filter.

The electrophoretic mobility of the particles after destabilization (level 1) was also monitored as a secondary parameter. A G.K. Turner Zeta Meter was employed to measure the mobility of the particles. The mobility measurement procedure consisted of recording the average mobility of ten particles found in each of the samples collected at half hour intervals. The ten particles were randomly selected to reflect the range of mobilities and particle sizes that were seen in the sample.

A list of all the pilot plant runs, including coagulant dosages and pH conditions can be found in Table 3. The total number of plant runs where coagulant was used was thirty-eight. An additional run without coagulant was also made in order to establish the filter's baseline removal efficiency. All the pilot plant runs were between three and five hours in length.

Table 3. List of Pilot Plant Runs Including Coagulant Dosages and pH Conditions.

COAGULANT DOSAGE/ COLLOID	MIXER	VELOCITY GRADIENT- $\bar{G}$ ( $s^{-1}$ )	NUMBER OF RUNS
Alum 8 mg/l @ pH 6.9 M30	Baffled	75	2
		210	2
		385	1
	Tank	810	2
		1640	2
		3000	1
		3800	2
Ferric Chloride 8 mg/l @ pH 6.2 M30	Baffled	75	2
		210	1
		810	1
	Tank	1640	1
		2290	2
		3000	1
		3800	2
Ferric Chloride 8 mg/l @ pH 6.3 SB325	Baffled	210	2
		810	2
		1640	2
	Tank	3000	1
		3800	1
Ferric Chloride 8 mg/l @ pH 6.2 M30	Hydraulic	705	1
		690	1
	Jump	680	1
		870	1
Ferric Chloride 8 mg/l @ pH 6.2 M30	Open	1080	1
		1360	1
	Channel	1700	1
		2300	1

Alum Dosage = 8 mg/l as  $Al_2(SO_4)_3 \cdot 14.3H_2O$

Ferric Chloride Dosage = 8 mg/l as  $FeCl_3 \cdot 6H_2O$

DYE TRACE STUDIES

In order to determine the macroscopic mixing characteristic of both the baffled tank and the hydraulic jump, standard dye trace studies were performed. By utilizing fluorometric techniques and common analysis procedures explained by Weber [29], a fairly good representation of the residence time distribution (RTD) for the given mixer was obtained. Weber also explains a numerical integration procedure which yields the centroid of the RTD. By definition, the centroid of the reactor RTD is the mean hydraulic residence time (MHRT) for the reactor. Furthermore, Weber illustrates a theoretical RTD calculation for a complete mix reactor.

Rhodamine WT, a nonreactive fluorescent dye, was used in the tracer studies. During the tracer studies, the dye was introduced into the mixers as a pulse, via the coagulant feed conduits. Samples were collected from the mixer effluent after the dye was injected and analyzed on a G.K. Turner Fluorometer. The fluorometer detected Rhodamine WT at concentrations as low as 0.0001 mg/l. The data from the fluorometer was later plotted and statistically analyzed as a described by Weber [29], to establish the mean hydraulic residence time for the given mixer.

## CHAPTER 6

## RESULTS AND DISCUSSION

The results of this investigation fall into three major categories. First, there is the calculated mixing parameters for the various mixers. Secondly, the pilot plant data and filtration results are considered. Finally, the hydraulic and mechanical mixer comparisons are made.

CALCULATED MIXING PARAMETERS

The parameters which were chosen to describe the mixing in the baffled tank and hydraulic jump were mean hydraulic residence time (MHRT) and the average mixer velocity gradient ( $\bar{G}$ ). For comparison purposes,  $\bar{G}t$  values have also been calculated. The value of  $t$  used was  $V/Q$  for the reactor. In regard to the hydraulic jump,  $t$  was assumed equal to the MHRT for the given jump. The methods for calculating the MHRTs and  $\bar{G}$ -values were outlined in the Previous Related Studies section and the following paragraphs focus on the results of the above mentioned calculations.

Velocity Gradients

Power dissipation within the baffled tank can be calculated by using the power number Equation (4) once the reactor power number is known. Leentvaar [8] reported that the

power number for a cylindrical baffled tank, with a disc impeller, was 5.0. It is important to note that power losses computed using the power number expression represent average losses within the entire tank volume. Thus, by using the power number losses in the expression for  $\bar{G}$ , Equation (2), an average velocity gradient for the baffled tank can be found. Table 4 lists the results of the power loss,  $\bar{G}$ -value and  $\bar{G}t$ -value calculations for the baffled tank.

Table 4. Calculated Velocity Gradients for Baffled Tank.

IMPELLER RPM	POWER DISSIPATION (ft·lbs/s)	VELOCITY GRADIENT- $\bar{G}$ (s <sup>-1</sup> )	$\bar{G}t$
50	0.02	75	3,900
100	0.18	210	10,900
150	0.62	385	20,000
250	2.74	810	42,100
400	11.21	1640	85,300
500	21.90	2290	119,100
600	37.84	3000	156,000
700	60.09	3800	197,600

$\bar{G}$ -values and  $\bar{G}t$  values for the hydraulic jump and open channel, for various channel slopes, are shown in Table 5. A sample calculation of the power loss and the  $\bar{G}$ -value for the jump can be found in the Appendix. It should be noted here that the open channel  $\bar{G}$ -value for the 3.5 inches per foot slope, may be in error. The reason for the error is related to the extreme curvature of the water surface in the flume at this large slope. Since the flume was only

Table 5. Calculated Velocity Gradients for Hydraulic Mixers.

	CHANNEL SLOPE (in/ft)	FROUDE NUMBER $F_1$	POWER DISSIPATION ft·lbs/s	$\bar{G}$ ( $s^{-1}$ )	$\bar{G}t$
HYDRAULIC JUMP	1.5	3.41	0.022	705	3595
	2.0	4.49	0.035	690	2970
	2.5	6.29	0.054	680	2920
	3.5	9.68	0.121	870	3480
OPEN CHANNEL	1.5	3.41	0.046	1080	530
	2.0	4.49	0.061	1360	550
	2.5	6.29	0.075	1700	550
	3.5	9.68	0.103	2300	560

1.0 inches wide, all the calculations had to be based on the center line depth. The curvature of the water surface may have thus yielded a low center line depth reading causing the calculated  $\bar{G}$ -value to be too high. None of the other channel slopes employed produced flows with extreme surface curvature.

In looking at the actual values for power dissipation for the jump, channel and baffled tank, it can be seen that the power requirements for the hydraulic mixers are significantly lower than the power requirements for the baffled tank.

#### Hydraulic Residence Times

The data collected from the dye trace studies was used to determine the residence time distributions for the baffled tank and the hydraulic jumps. Figure 9 represents the RTDs for three different impeller speeds in the baffled tank.

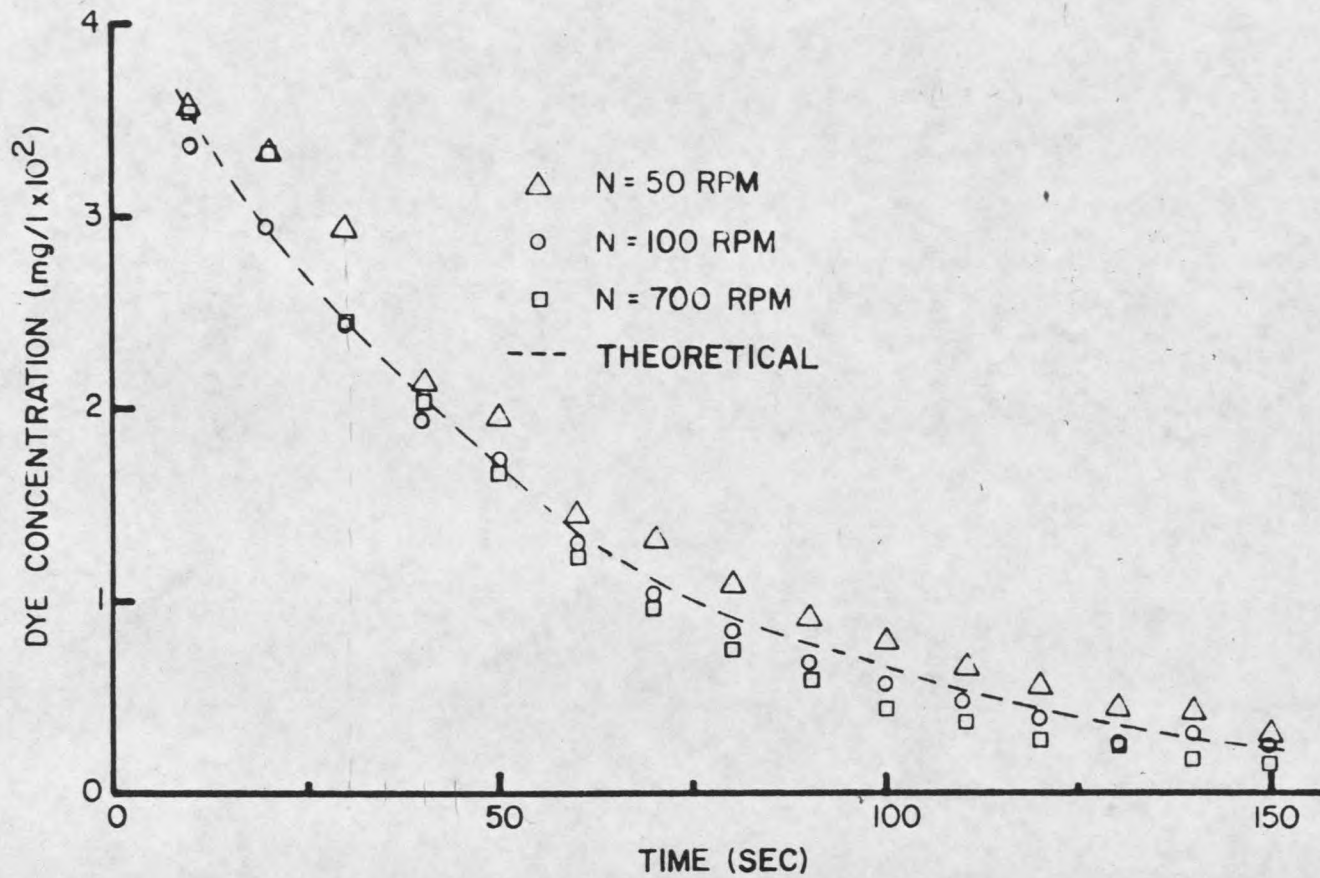


FIGURE 9. Residence Time Distributions for the Baffled Tank Reactor.

The RTDs do not seem to be particularly dependent on the impeller speed and all the data follows the theoretical curve derived from a mass balance across the reactor [27]. However, the mean hydraulic residence times (centroid of distribution) for each of the impeller speeds, listed in Table 6, are significantly different. Note that changes in the dye concentration within the baffled tank during the first ten seconds were not included in the numerical integration procedure used to obtain the MHRTs listed in Table 6.

Table 6. Mean Hydraulic Residence Times for Baffled Tank.

IMPELLER RPM	MEAN HYDRAULIC RESIDENCE TIME (Seconds)
50	65.6
100	56.6
700	50.3

Reactor Volume/Flow Rate = 52.0 seconds

Two typical RTDs for the hydraulic jumps are shown in Figure 10. In comparison to the baffled tank RTDs discussed above, two important differences are evident. First, the hydraulic jump RTDs are more closely centered about their respective MHRTs (plug-flow). Also, the average mixing time or MHRT for the hydraulic jumps is about an order of magnitude less than the tank MHRTs (4-5 second MHRT for all jumps). Thus, the macroscopic mixing in the hydraulic jumps and the baffled tank used in the experiments are vastly different.

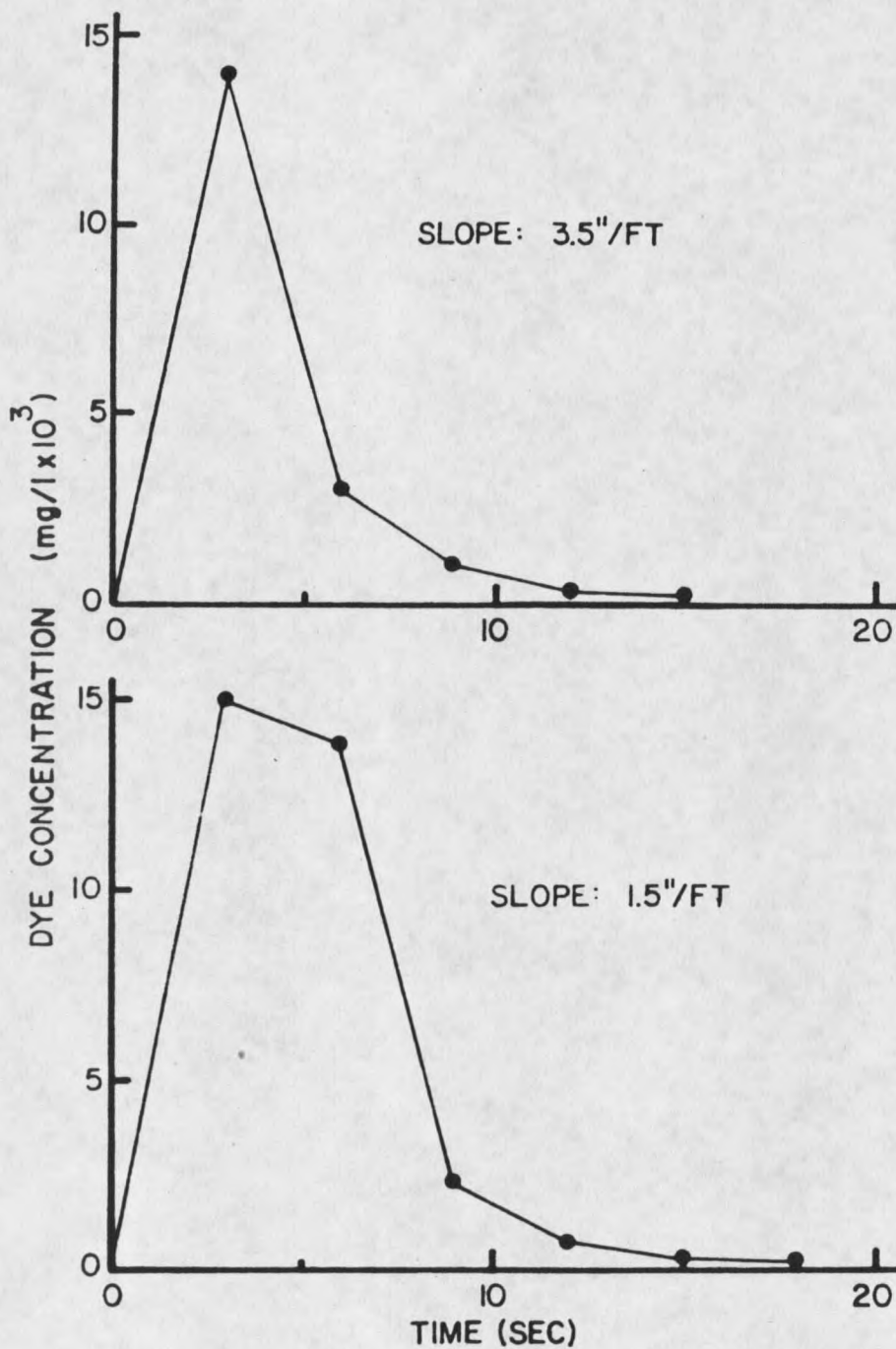


FIGURE 10. Residence Time Distributions for Two Hydraulic Jumps.

## FILTRATION RESULTS

As outlined in the Experimental Work section, the raw filter data consisted of various turbidity and headloss readings. The turbidity data will be referenced directly by the level (1-6) from which the sample was taken. Headloss data on the other hand, is coded by referring to the levels through which the loss occurred. For example, the headloss in the uppermost layer of coal would be H1-2 and the total headloss would be H1-6 (see Figure 8).

Two typical examples of raw filter data are shown in Figures 11 and 12. The top graph in each figure shows the turbidity removal as a function of time and the lower graph illustrates the corresponding headlosses. Note that the headloss lines are very linear, which is characteristic of a stable well designed filter system with good depth removal. A single plant run was also made in which no coagulant was added. This no treatment run was performed in order to establish a base for the other plant runs. The results of the no coagulant run showed that the filter would not remove any of the nondestabilized material. This also led to a zero headloss buildup.

### Filter Response to Baffled Tank Mixing

As a first attempt to define the effectiveness of various mixing conditions for the baffled tank, the rate of headloss buildup and average effluent turbidity for each run was

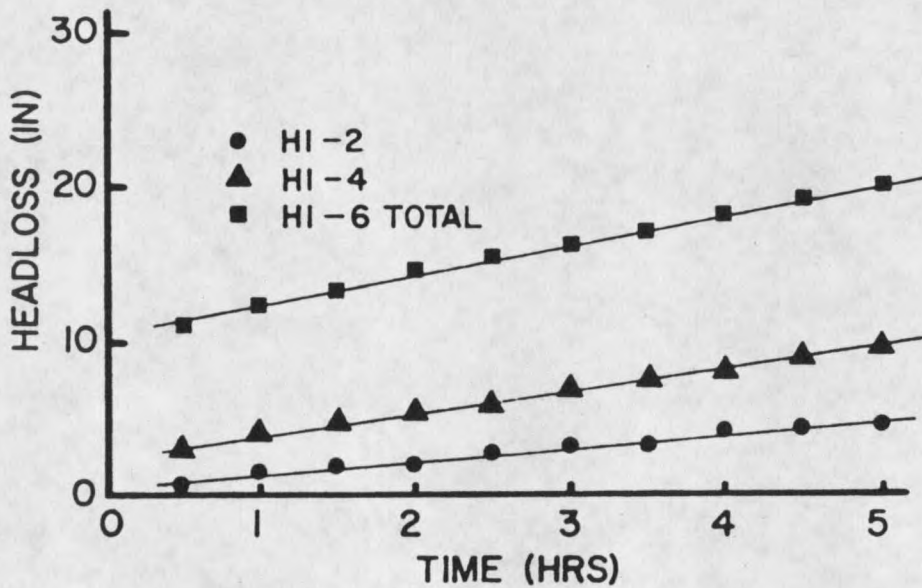
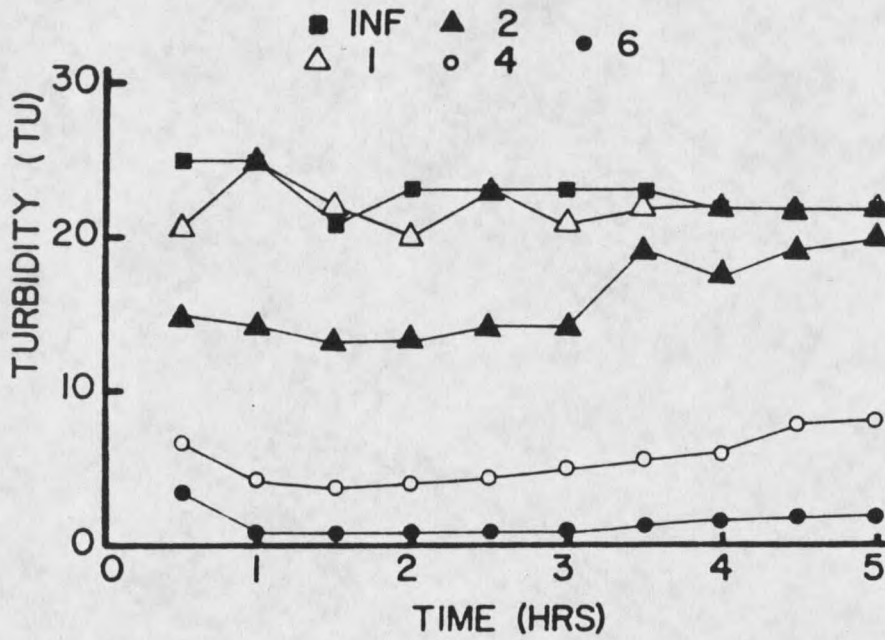


FIGURE 11. Typical Filter Data for Ruffled Tank Mixing with Alum Treatment ( $n = 700$  RPM).

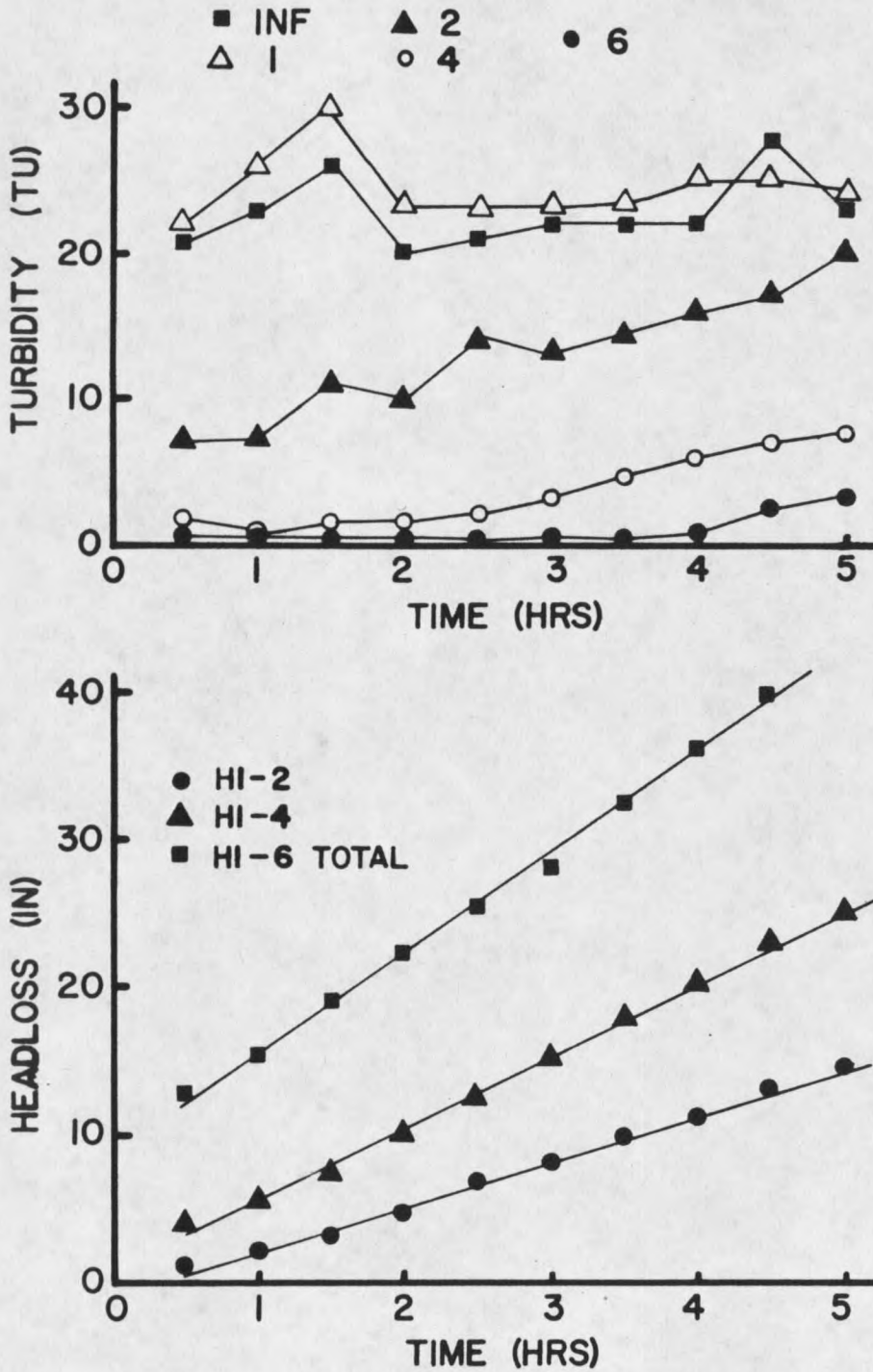


FIGURE 12. Typical Filter Data for Hydraulic Jump Mixing with Ferric Chloride Treatment (slope = 2.0 in/ft).

calculated and compared. The rate of headloss is simply the slope of the linear headloss lines which were illustrated in Figures 11 and 12. Rates of headloss were calculated for various plant runs by performing linear regressions on the headloss data. Average effluent turbidity is defined herein as the average of all the effluent turbidity readings up to and including a specified breakthrough turbidity ( $\bar{C}$ ). The breakthrough turbidity was used to determine the run length,  $T$ , and was set at 1.5 TU for M30 suspensions and 1.0 TU for SB325 suspensions. In other words, when the effluent turbidity of a given plant run reached the appropriate breakthrough turbidity value, the run was terminated.

The rates of headloss development and average effluent turbidity for alum treatment of the M30 suspension are shown in Figure 13. The rates of headloss do not vary significantly above a  $\bar{G}$  of approximately  $800 \text{ s}^{-1}$ , however, a minimum rate seems to have been reached at a  $\bar{G}$  of  $3000 \text{ s}^{-1}$ . Correspondingly, the average turbidity for alum treatment did not vary significantly with velocity gradient. The insensitivity of the data shown in Figure 13 seemed unreasonable, and was most likely related to the sulfates in the influent water. In order to avoid the sulfate problem, the coagulant was changed to ferric chloride and the experiments were repeated.

Figure 14 illustrates the rates of headloss for ferric chloride treatment of the M30 suspension. All trends in

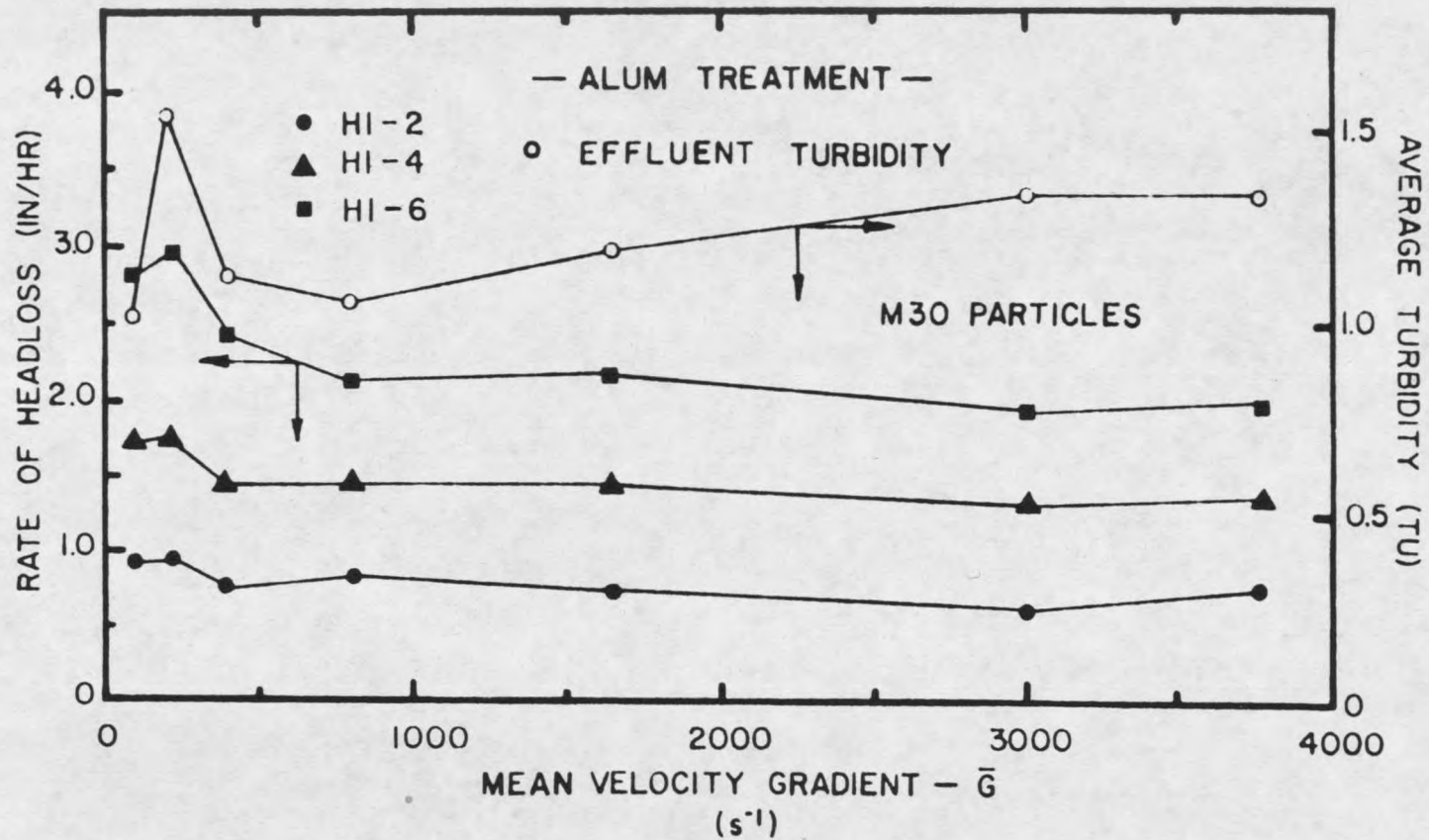


FIGURE 13. Rates of Headloss and Average Effluent Turbidities for Baffled Tank Mixing with Alum Treatment.

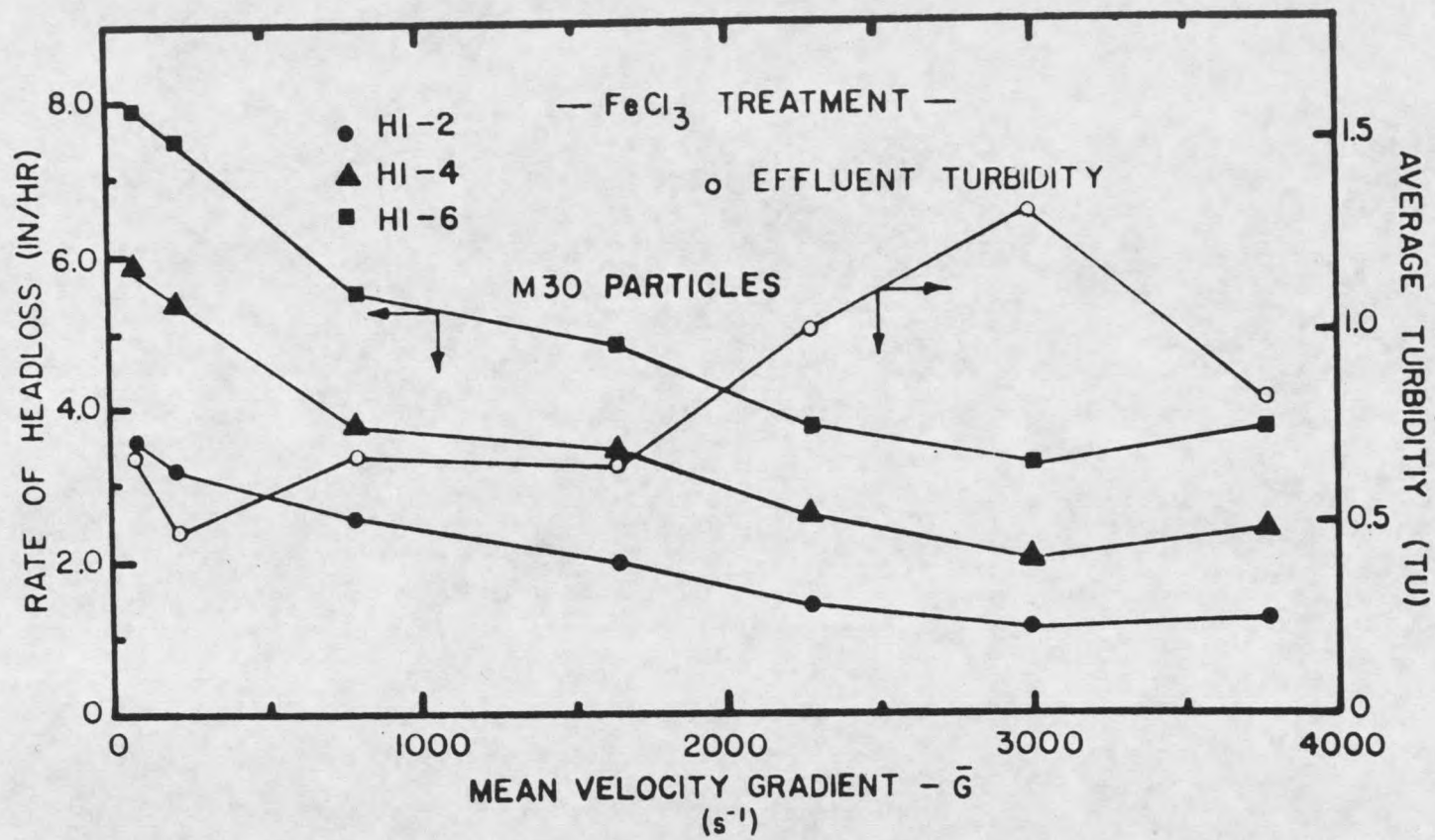


FIGURE 14. Rates of Headloss and Average Effluent Turbidities for Baffled Tank Mixing with Ferric Chloride Treatment.

Figure 14 are similar to the trends for alum treatment; however, note the 100% change in the rate of headloss and near 300% change in the average turbidity over the  $\bar{G}$ -value range shown. As a result of the increased sensitivity of the ferric chloride system, no further alum treatment experiments were performed.

The SB325 suspension was also treated with ferric chloride and the resulting headloss rates and corresponding turbidities are shown in Figure 15. Once again, the rate of headloss changes significantly over the velocity gradient range employed, with high  $\bar{G}$ -values producing lower rates of headloss. The average effluent turbidities are somewhat less sensitive to changes in mixing for the SB325 suspension in comparison to turbidities for the M30 suspension. The lower sensitivity was actually expected, since on a mass basis (mg/l), a finer distribution of colloids will produce higher turbidities (light scattering) than a coarser distribution.

It was evident from Figures 13 through 15, that no clear cut optimum condition could be identified because the headloss and turbidity data opposed each other. Thus, it became necessary to combine headloss and turbidity data into a single filtrability index in order to pinpoint possible optimum mixing conditions. Also, correlations between the turbulent microscale and the colloid distributions could

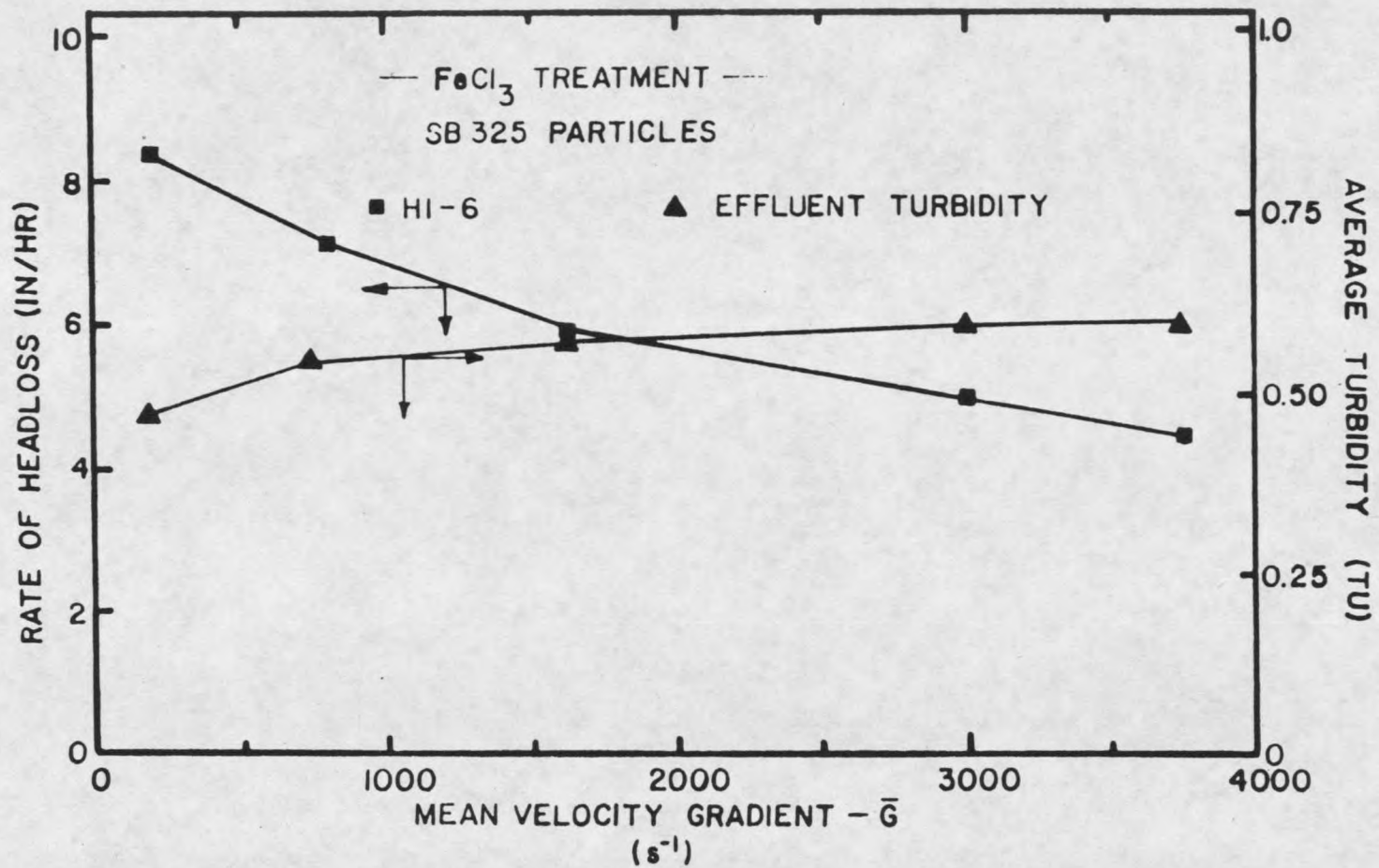


FIGURE 15. Rates of Headloss and Average Effluent Turbidities for Baffled Tank Mixing with Ferric Chloride Treatment.

probably not be identified unless a single parameter was used to describe the filter response.

#### Filtrability Numbers for Baffled Tank Mixing

Filtrability numbers for various plant runs were calculated using Equation (9) and plotted against average reactor velocity gradients. The filtrability numbers obtained are shown in Figures 16 through 18. Also plotted in Figures 16 through 18 are the turbulent microscales for the impeller stream zone (see Appendix). Figure 16 is for alum treatment of the M30 suspension and the expected insensitivity is evident. Figures 17 and 18, on the other hand, illustrate once again that the ferric chloride system provides much more information in regard to the filter's response to various degrees of mixing. Since larger filtrability numbers are indicative of poorer filtration conditions, Figures 17 and 18 seem to indicate that relative minimum filtration conditions exist for both the M30 and the SB325 distributions.

Looking back at the grain size distributions for M30 and SB325, shown in Figure 5, it can be seen that the mean particle size for M30 and SB325 distributions (number count) is approximately 3.0  $\mu\text{m}$  and 6.0  $\mu\text{m}$  respectively. According to the mixing interaction model developed herein, minimum interactions (filtration conditions) should exist when the turbulent microscales are twice the colloid size. Thus,

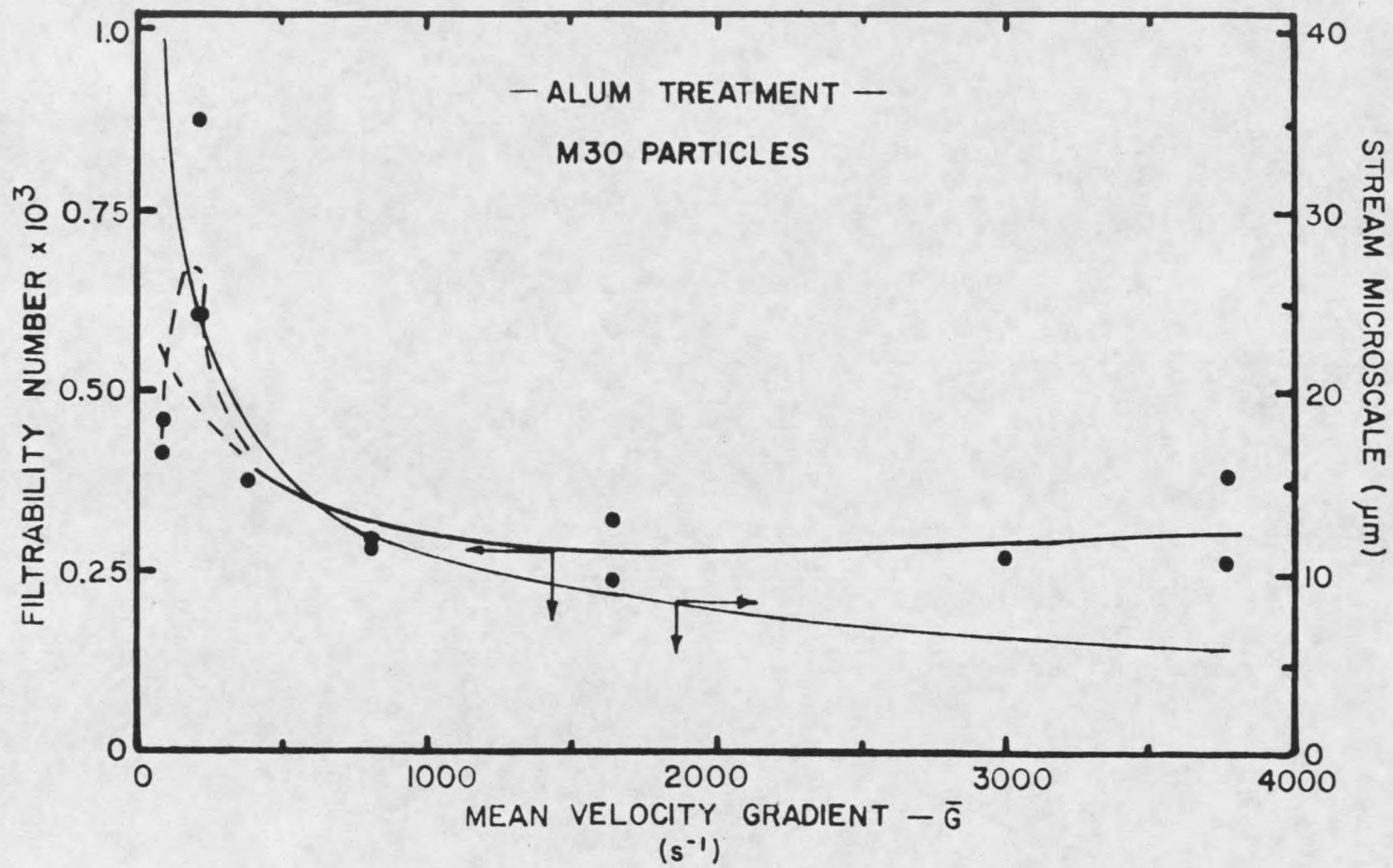


FIGURE 16. Filtrability Numbers for Ruffled Tank Mixing with Alum Treatment.

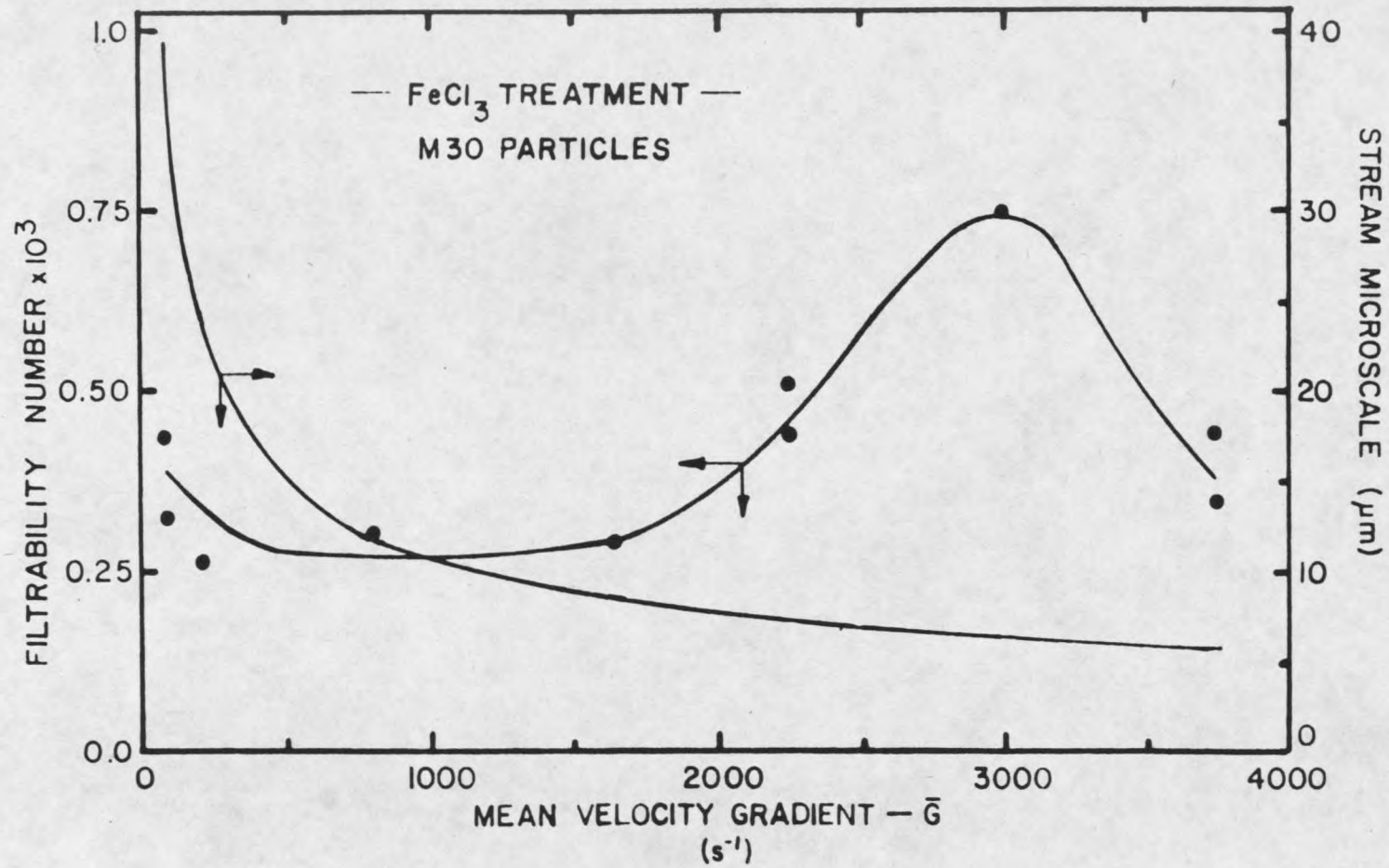


FIGURE 17. Filtrability Numbers for Ruffled Tank Mixing with Ferric Chloride Treatment.

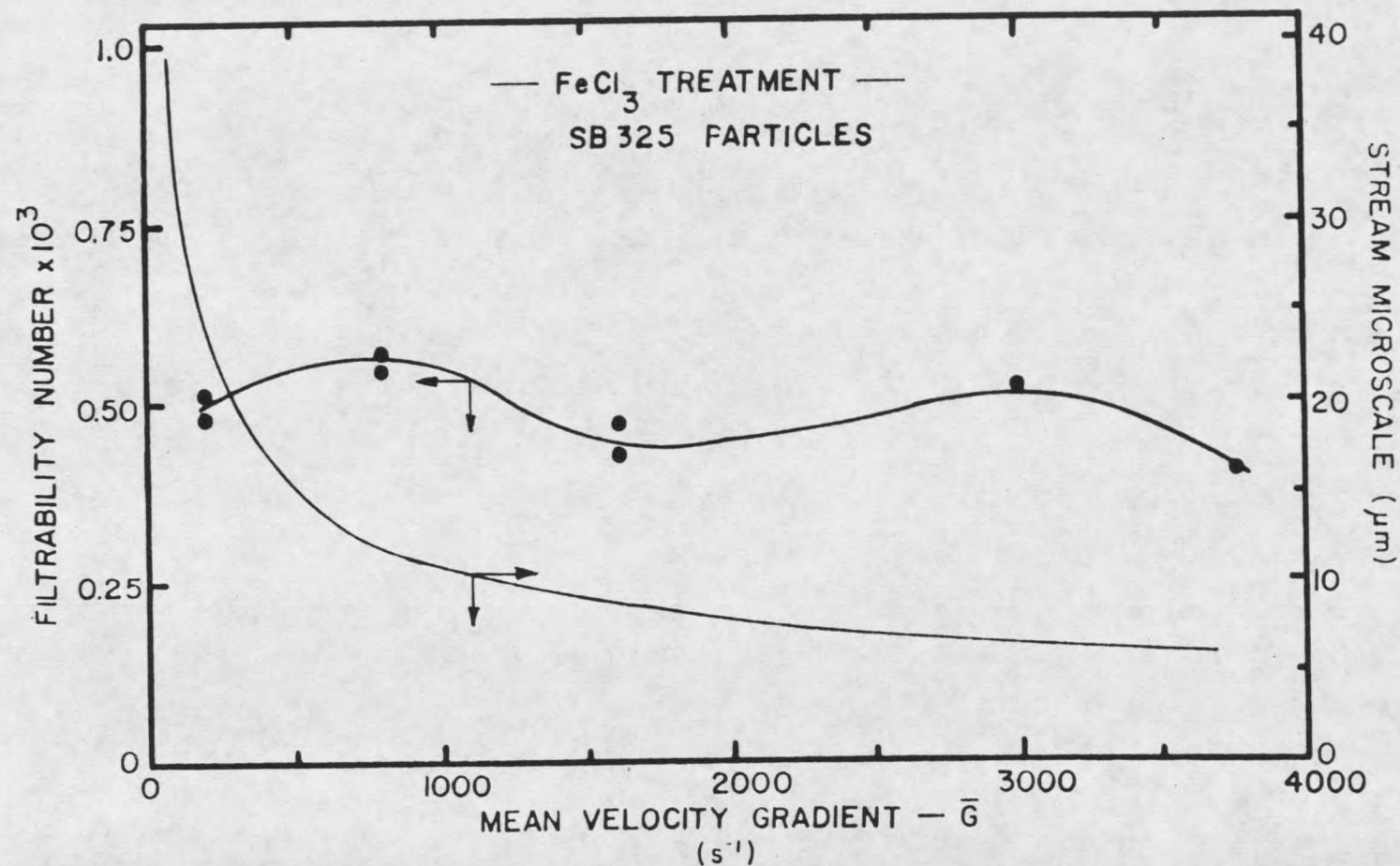


FIGURE 18. Filtrability Numbers for Baffled Tank Mixing with Ferric Chloride Treatment.

for the M30 and SB325 distributions, minimum filtration conditions should exist when the microscales are approximately 6 and 12  $\mu\text{m}$  respectively. The preceding statement assumes, of course, that the colloid distribution can be represented by its mean size. The 6 and 12  $\mu\text{m}$  microscales correspond to velocity gradients of  $3000 \text{ s}^{-1}$  and  $810 \text{ s}^{-1}$ . Inspection of Figures 17 and 18 show that minimum filtration conditions for the experimental systems occur at stream microscales very close to 6  $\mu\text{m}$  for M30 and 12  $\mu\text{m}$  for SB325. Recalling that the coagulant was introduced into the baffled tank in the impeller stream, a microscale-colloid size correlation in the stream region would seem the most reasonable.

A secondary minimum filtration condition is also shown in Figure 18 ( $\bar{G}=3000$ ). This secondary minimum is most likely related to the fraction of small particles in the SB325 distribution which are of size 3.0  $\mu\text{m}$ ; these small particles have the greatest impact on the measurement of turbidity.

#### ELECTROPHORETIC MOBILITY DATA

Recall that the electrophoretic mobility of the destabilized (level 1) suspension was also measured regularly throughout each plant run. Each recorded mobility was, in actuality, the average mobility for ten particles, and thus, between 60 and 90 particle mobilities were measured during a given run. Table 7 lists the average mobilities

obtained from the various mixing conditions employed to treat the M30 and SB325 suspensions. It can be seen from Table 7 that the highest mobilities occur at, or very close to, the microscale-colloid size correlation points discussed in the previous section. Although the mobility data seems somewhat scattered, any conclusion which is drawn from the mobility measurements is supported by the large number of samples which make up the average values. In fact, statistical analysis of the mobility data yielded 95% confidence intervals which were so small, that the intervals could be considered insignificant. Thus, both the mobility data and filtrability numbers seem to suggest the existence of a size correlation between the turbulent microscale and the mean size of the colloid distribution.

#### HYDRAULIC MIXER COMPARISONS

Comparing hydraulic mixing to baffled tank mixing was handled by utilizing the velocity gradient concept. Within the context of this investigation, comparing mixers from a  $\bar{G}$ -value standpoint answered two related questions. First, the comparisons gave some insight into whether the proposed method for calculating  $\bar{G}$ -values for hydraulic jumps was reasonable. Secondly, comparisons based on  $G$  established the jumps mixing effectiveness in relation to the effectiveness of the baffled tank. It should be noted here that a similar

Table 7. Electrophoretic Mobility Data for Treatment of M30 and SB325 Colloids

CONDITIONS	VELOCITY GRADIENT ( $s^{-1}$ )	ELECTROPHORETIC* MOBILITY MEAN $\pm$ 95% C.I. ( $\mu m \cdot cm/volt \cdot s$ )
Alum Treatment of M30 Particles	75	0.90 $\pm$ 0.02
	210	1.01 $\pm$ 0.04
	385	1.00 $\pm$ 0.02
	810	0.94 $\pm$ 0.02
	1640	0.98 $\pm$ 0.01
	3000	1.15 $\pm$ 0.03
	3800	1.16 $\pm$ 0.04
Ferric Chloride Treatment of M30 Particles	75	1.22 $\pm$ 0.02
	210	1.21 $\pm$ 0.02
	810	1.09 $\pm$ 0.01
	1640	1.19 $\pm$ 0.03
	2290	1.27 $\pm$ 0.02
	3000	1.31 $\pm$ 0.03
	3800	1.11 $\pm$ 0.03
Ferric Chloride Treatment of SB325 Particles	210	1.60 $\pm$ 0.03
	810	1.52 $\pm$ 0.04
	1640	1.70 $\pm$ 0.02
	3000	1.55 $\pm$ 0.04
	3800	1.44 $\pm$ 0.03

\*Non destabilized particle mobility = 2.2  $\mu m \cdot cm/volt \cdot s$

$\bar{G}$ -value for the jump and tank does not imply a similar  $\bar{G}t$  value. In fact, for a given  $\bar{G}$  (600-900  $s^{-1}$ ) the  $\bar{G}t$  values for the hydraulic jump are an order of magnitude smaller than than the  $\bar{G}t$  values for the baffled tank.

The rates of headloss of both hydraulic mixers (jump and channel) are shown in Figure 19. The data in Figure 19 indicates that the rates of headloss produced in the filter

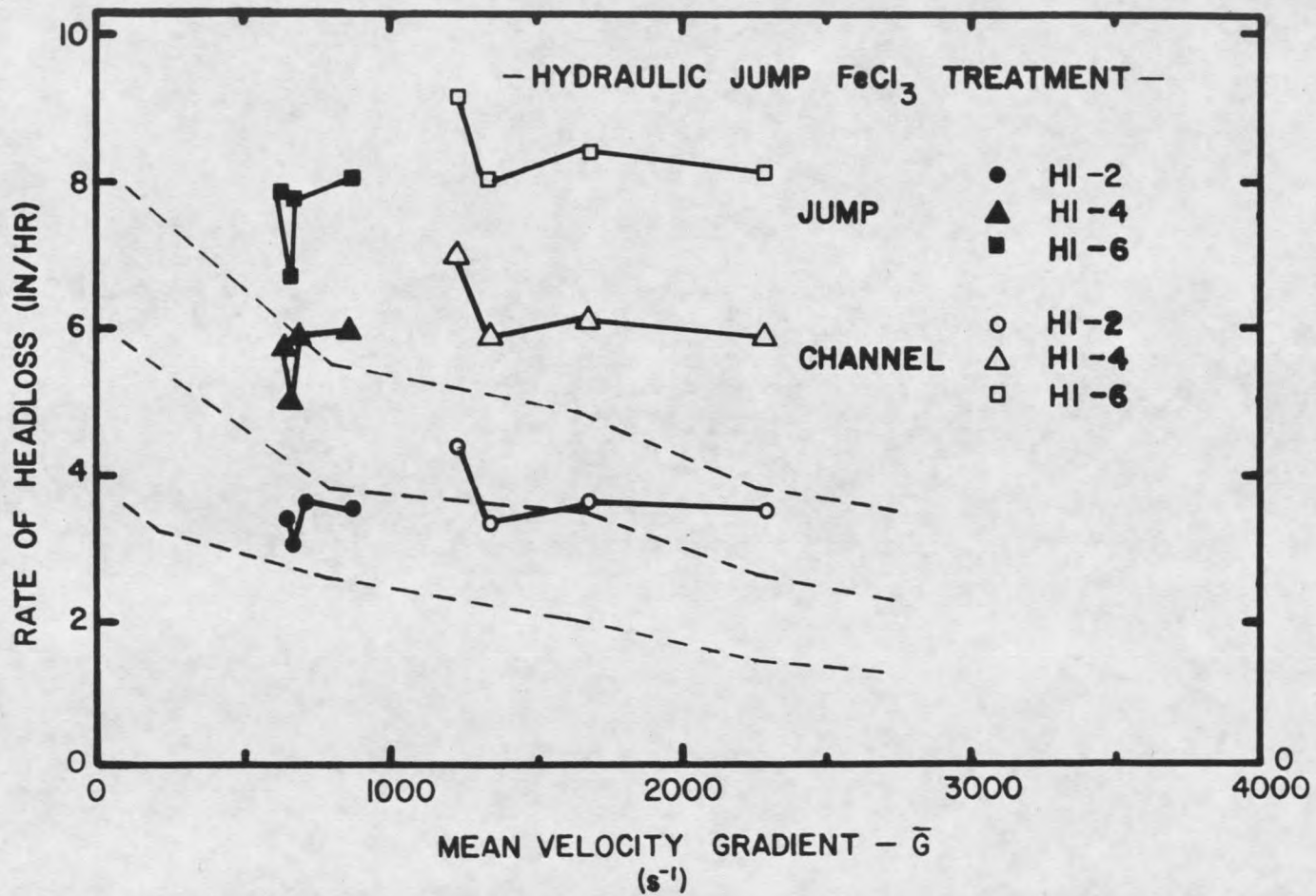


FIGURE 19. Rates of Headloss for Hydraulic Jump and Open Channel Mixing with Ferric Chloride Treatment.

for both the jump and the channel are higher than the rates which resulted from baffled tank mixing. At first glance, Figure 19 might suggest that the  $\bar{G}$ -values for the jump were too large since the hydraulic and mechanical data would align if the jump  $\bar{G}$ -values were less. However, the velocity gradient calculation for open channel mixing is well defined, yet the channel data as well, does not align with the baffled tank data.

From a turbidity standpoint, Figure 20 indicates that the hydraulic mixers produced a slightly higher quality effluent than the baffled tank. Thus, the increased headloss depicted in Figure 19 was understandable.

Combining the headloss and turbidity data to form corresponding filtrability numbers leads to the comparison illustrated in Figure 21. The filtrability data tends to support the  $\bar{G}$ -value calculation method since the baffled tank and jump data are in good agreement. Furthermore, Figure 21 indicates that the hydraulic jump and open channel are equally as effective as the baffled tank in regard to rapid mixing of chemical coagulants. Once again, it should be noted that the actual power dissipations in the hydraulic mixers were significantly less than the power dissipations for the baffled tank.

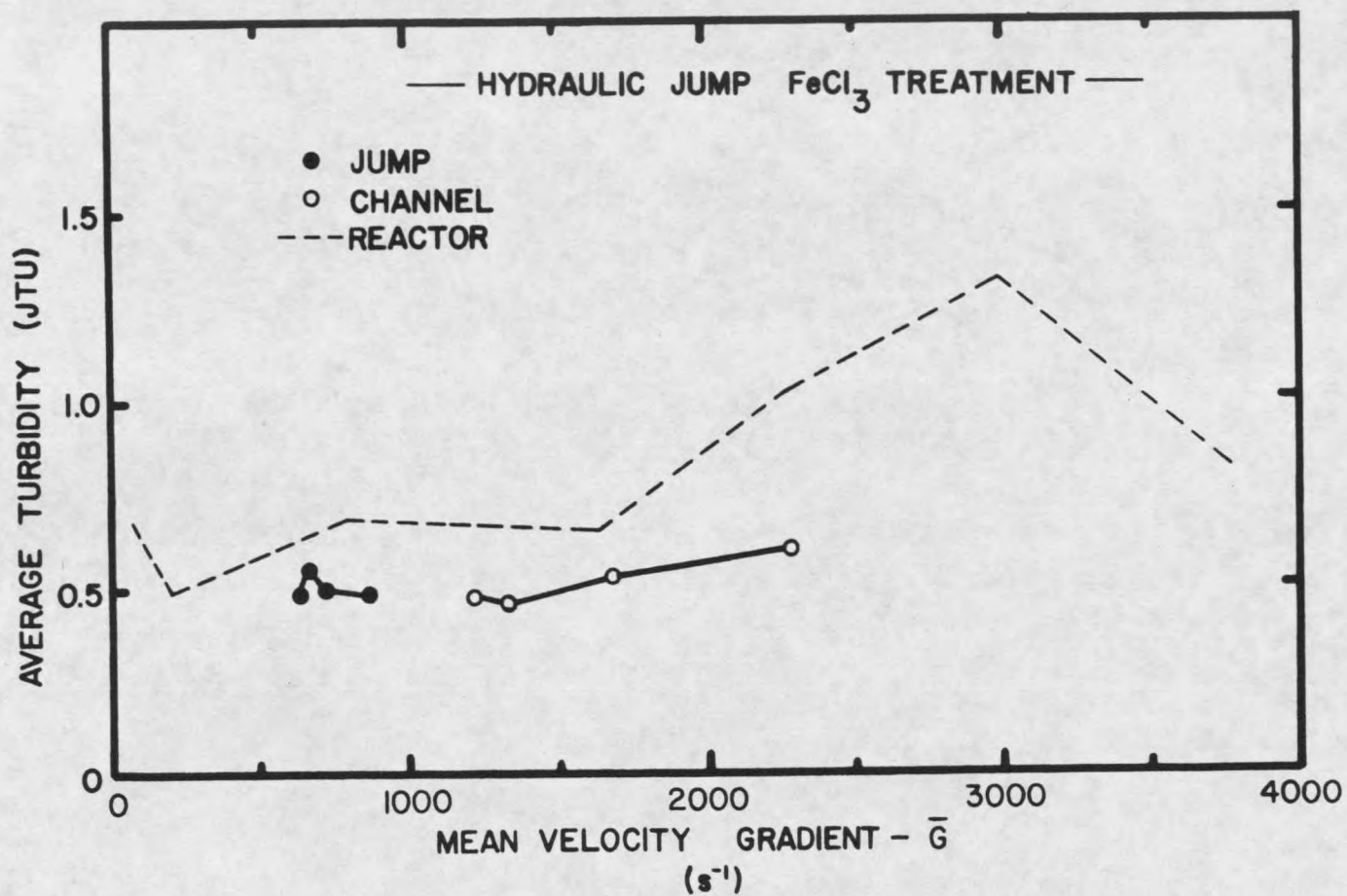


FIGURE 20. Average Effluent Turbidities for Hydraulic Jump and Open Channel Mixing with Ferric Chloride Treatment.

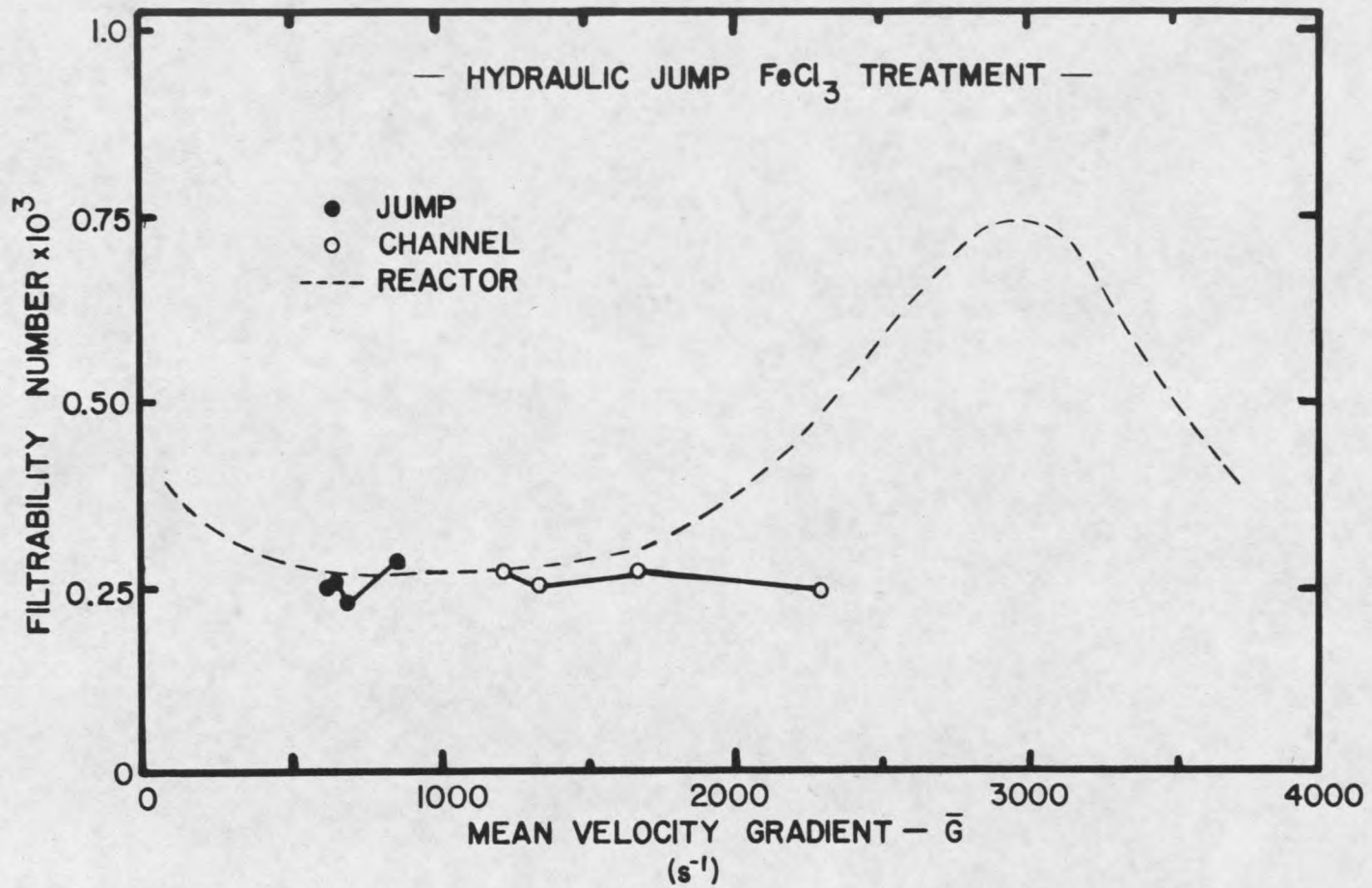


FIGURE 21. Filtrability Numbers for Hydraulic Jump and Open Channel Mixing with Ferric Chloride Treatment.

## CHAPTER 7

## CONCLUSIONS

Based on the results of this study, the following conclusions can be drawn:

1. A size correlation between the turbulent microscale and the colloid distribution seemed to exist for the rapid mixing process of coagulation. The existence of this correlation was supported by pilot plant filtration data as well as particle electrophoretic mobility data.
2. The microscale-colloid interaction model proposed herein may provide some insight into the size correlation mentioned above. The mixing model may not actually define the physical nature of the rapid mixing process, however, the model seems to predict the minimum interaction condition for the mixer used in this study.
3. In regard to optimum mixing conditions, the data collected indicates that the size of the colloid suspension being treated must be considered before optimum conditions can be defined. The filtrability data indicated that average velocity gradients from 700 to 1500  $s^{-1}$  or, possibly gradients above 4000  $s^{-1}$ , were best for the

particle suspension used in this study.

4. Use of the hydraulic jump design procedure developed here resulted in  $\bar{G}$ -values which were reasonable and functionally correct. Although the procedure developed here was for jumps occurring in sloping channels, a similar methodology could be developed for jumps occurring downstream of a critical flow flume.
5. In the average velocity gradient range of 600 to 900  $s^{-1}$ , the mixing effectiveness of the hydraulic jump was found to be equal to that of the baffled tank. Furthermore, because of the difference in the size of the power dissipation volumes of the jump and the tank, significantly less power was required to produce the above  $\bar{G}$ -values in the hydraulic jump.
6. The inflexibility of a hydraulic jump as a mixer was also very apparent. In spite of the attempts made in this study to produce jumps of variable velocity gradient, all the jumps fell within a narrow  $G$ -value range. It is this inflexibility that will continue to limit the use of the hydraulic jump in mixing operations.

## REFERENCES

1. Hinze, J.O. Turbulence. 2nd ed. New York:McGraw Hill, 1975.
2. Bradshaw, P. An Introduction to Turbulence and its Measurement. New York:Pergamon Press, 1971.
3. Kolmogoroff, A.N. "The Local Structure of Turbulence in Incompressible Viscous Fluid for Very Large Reynolds Numbers." C.R. Acad. Science U.R.S.S. 31 (1941):518.
4. Kolmogoroff, A.N. "On Degeneration of Isotropic Turbulence in an Incompressible Viscous Liquid." C.R. Acad. Science U.R.S.S. 31 (1941):538.
5. Cutter, Louis, A. "Flow and Turbulence in a Stirred Tank." American Institute of Chemical Engineers Journal 12 (January, 1966):35-45.
6. Okomoto, Y., Nishikawa, M. and Hashimoto, K. "Energy Dissipation Rate Distribution and its Effects on Liquid-Liquid Dispersion and Solid-Liquid Mass Transfer." International Chemical Engineering 21 (January 1981):88-94.
7. Camp, T.R. and Stein, P.C. "Velocity Gradients and Internal Work in Fluid Motion." Journal of the Boston Society of Civil Engineers 30 (1943):219-237.
8. Leentvaar, J. and Ywema, T.S.J. "Some Dimensionless Parameters of Impeller Power in Coagulation-Flocculation." Water Research 14(1980):135-140.
9. Chow, V.T. Open Channel Hydraulics. New York:McGraw Hill, 1953.
10. Wilson, G.E. "Initial Mixing and Turbulent Flocculation" Ph.D. dissertation, University of California, 1972
11. Stenquist, R.J. and Kaufman, W.J. Initial Mixing in Coagulation Processes. U.S. Environmental Protection Agency, EPA-R2-72-053, (1972).

12. Amirtharajah, A. and Mills, K.M. "Rapid-Mix Design for Mechanisms of Alum Coagulation." Journal of the American Water Works Association 74 (April 1982): 210-216.
13. Amirtharajah, A. "Initial Mixing." American Water Works Association, Seminar Proceedings, Coagulation and Filtration: Back to the Basics. St. Louis, MO, 1981.
14. Levy, A.G. and Ellms, J.W. "The Hydraulic Jump as a Mixing Device." Journal of the American Water Works Association 17 (January 1927):1-23.
15. Smoluchowski, M. Physical Chemistry 92 (1917):129.
16. Saffman, P.G. and Turner, J.S. "On the Collision of Drops in Turbulent Clouds." Journal of Fluid Mechanics 16 (1956):16-30.
17. Spielman, L.A. "Hydrodynamic Aspects of Flocculation" The Scientific Basis of Flocculation (K.J. Ives, editor) Netherlands:Sijthoff and Noordhoff, 1978.
18. Adler, P.M. "Hetrocoagulation in Shear Flow." Journal of Colloid and Interface Science 83 (September 1981):106-115.
19. Gamet, M.B. and Rademacher, J.M. "Measuring Filter Performance." Water Works Engineering 112 (1959): 117-149.
20. Cleasby, J.L. "Approches to a Filtrability Index for Granular Filters." Journal of the American Water Works Association 61 (August 1969):372-381.
21. Ives, K.J. "A New Concept on Filtrability." Prog. Water Technology 10 (1978):123-137.
22. Bisker, C.D. and Young, J.C. "Two-Stage Filtration of Secondary Effluent." Journal of the Water Pollution Control Federation 69 (February 1977):319-351.
23. Lekkas, T.D. "A Modified Filtrability Index for Granular Bed Water Filters." Filtration and Separation 18 (May/June 1981):214-216.

24. Janssens, J.G., Adam, C. and Buekens, A. "Statistical Analysis of Variables Affecting Direct-Filtration" European Federation of Chemical Engineers, Proceedings of the International Symposium on Water Filtration. Antwerp, Belgium:1982.
25. Amirtharajah, A., Personal communication, May 1982.
26. Baumann, E.R. Chapter 2 "Granular-Media Deep-Bed Filtration" Water Treatment Plant Design (R.L. Sanks, editor) Ann Arbor:Ann Arbor Science Publishers, 1978.
27. Letterman, R.D. and Vanderbrook, S.G. "Effect of Solution Chemistry on Coagulation with Hydrolyzed Al(III):Significance of Sulfate Ion and pH." Water Research 17 (1983):195-204.
28. Amirtharajah, A. Chapter 28 "Design of Granular-Media Filter Units." Water Treatment Plant Design (R.L. Sanks, editor) Ann Arbor:Ann Arbor Science Publishers, 1978.
29. Weber, W.J. Physicochemical Process for Water Quality Control. New York:Wiley and Sons, 1972.

APPENDIX

SAMPLE CALCULATIONS

1. Hydraulic jump velocity gradient.

Measurements of depth and elevation within the flume led to the following data for the 1.5 inches per foot slope.

$$\begin{aligned} E_T &= 0.078 \text{ ft} & y_2 &= 0.128 \text{ ft} \\ F_1 &= 3.42 & S &= \sin \theta = 0.124 \end{aligned}$$

The power dissipated in the jump can then be found using Equation (7) where

$$\gamma = 62.2 \text{ lbs/ft}^3 \text{ (80}^\circ\text{F)} \quad Q = 2.0 \text{ gpm} = 4.46 \times 10^{-3} \text{ cfs}$$

$$\bar{P} = \gamma Q(E_T)$$

Using  $F_1$ ,  $y_2$  and  $S$  in Figure 22 yields a jump length:

$$L = 0.461 \text{ ft}$$

Thus, the dissipation volume,  $V$ , is approximated by a triangular wedge of 1.0 inch width or

$$V = 1/2 L y_2 (0.083) \text{ ft}^3$$

Finally, substitution into equation (2) where

$$\mu = 1.799 \times 10^{-3} \text{ lb}\cdot\text{s/ft}^2$$

$$\bar{G} = 705 \text{ s}^{-1}$$

The above  $\bar{G}$ -value being an approximation of the velocity gradient for the hydraulic jump generated on the 1.5 inches per foot slope.

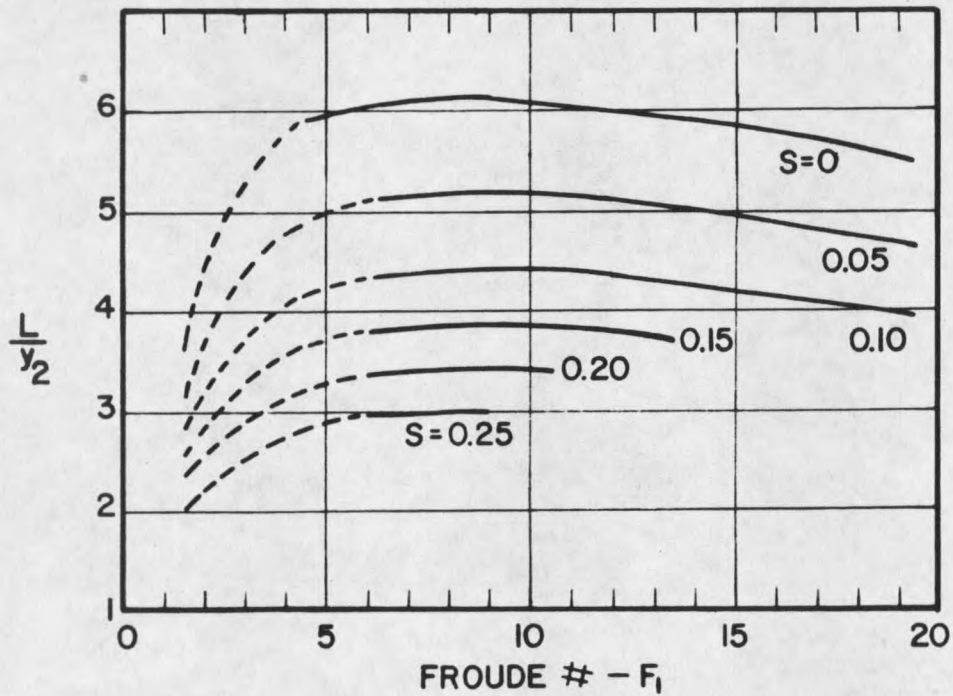
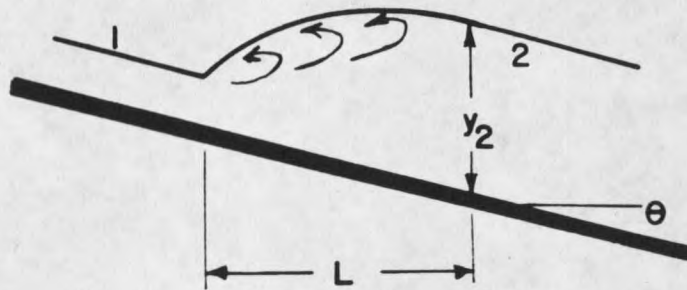


FIGURE 22. Hydraulic Jump Length,  $L$ , for Jumps in Sloping Channels.

## 2. Impeller stream microscale

Taking the case for a velocity gradient of 3000  $s^{-1}$ , Table 3 lists an average power dissipation of 37.84 ft·lb/s. Referring to Figure 1, the approximate power dissipation in the impeller stream would be

$$P_{m2} = 5.4 (37.84) = 204.3 \text{ ft}\cdot\text{lb/s}$$

Converting  $P_{m2}$  to the power dissipation per unit mass is accomplished by realizing that

$$\epsilon = \left( \frac{P_{m2}}{\rho V_2} \right)$$

where

$$\rho = 1.934 \text{ slugs/ft}^3 \text{ and } V_2 = 0.095V = 0.022 \text{ ft}^3$$

thus

$$\epsilon = 4792.9 \text{ ft}^2/\text{s}^3$$

Substituting into Equation (1) where

$$\nu = 9.3 \times 10^{-6} \text{ ft}^2/\text{s} \text{ (80°F)}$$

$$\eta = 2 \times 10^{-5} \text{ ft} = 6.2 \text{ }\mu\text{m}$$

MONTANA STATE UNIVERSITY LIBRARIES  
stks N378.T776@Theses  
Turbulent rapid mixing in direct filtrat RL  
3 1762 00163740 2



MAINT

N378  
T776  
cop.2

Trusler, S. L.  
Turbulent rapid mixing  
in direct filtration

DATE	ISSUED TO
	<b>3 WKS USE INTERLIBRARY LOAN</b>
8/20/81	5127167
	<b>3 WKS USE INTERLIBRARY</b>

N378  
T776  
cop 2